Geological Quarterly, 2022, 66: 28
DOI: http://dx.doi.org/10.7306/gq.1661

Stacked Gilbert-type deltas filling an incised palaeovalley along the cratonward margin of a foreland basin (Miocene, Western Carpathian Foredeep)

Slavomír NEHYBA[1, *]

[1] Department of Geological Sciences, Faculty of Science, Masaryk University, Kotlářská 2, CZ- 611 37 Brno, Czech Republic

Nehyba, S., 2022. Stacked Gilbert-type deltas filling an incised palaeovalley along the cratonward margin of a foreland basin (Miocene, Western Carpathian Foredeep). Geological Quarterly, 2022, 66: 28, doi: 10.7306/gq.1661

Associate Editor: Anna Wysocka

The coarse-grained Brno sands are an important groundwater aquifer and represent a volumetrically significant component of the Lower Badenian/Middle Miocene sedimentary infill of the Western Carpathian Foredeep, a foreland basin formed on the eastern margin of the Bohemian Massif in front of the Western Carpathians. The integration of core and outcrop facies analysis, summary of facies features, depositional processes and architectures, and integration of provenance analysis have led to a new depositional model for the Brno sands as the product of Gilbert-type delta systems prograding into an incised palaeovalley developed on the outer foreland basin margin. The position, shape and morphology of the palaeovalley were influenced by pre-Neogene basement faults trending NW–SE. The Gilbert-type deltas recognized can be classified as foreset-dominated with other elements subordinate. The foreset beds mainly reflect low-density turbidites, with varied but important evidence of deposits of high-density turbidity currents, cohesionless debris flows and debris falls. The thick foreset deposits show, in detail, repetitive successive prograding-retrograding episodes. These are interpreted as rapid high-frequency pulses of relative sea level change i.e. as high-frequency depositional sequences. The deltaic deposition of the Brno sands was terminated by deposits of a shoal-water delta and the sands were finally drowned by a thick pile of offshore pelagic clays. The provenance of Brno sands is located into the nearby geological units. Redeposition from the older basin infill also played an important role.

Key words: Western Carpathian Foredeep, incised valley, Gilbert-type deltas, stratigraphic architecture, provenance analysis.

INTRODUCTION

Palaeovalleys which dissected the foreland plate of foreland basin provide unique information about flexurally induced sea level changes, the foreland palaeodrainage network and the role of external factors (climate, tectonics, sediment supply and palaeomorphology) in influencing the architecture of the basin infill. They usually have good potential to indicate allogenic and autogenic factors and constitute basic data for interpreting the stratigraphic organisation of sedimentary basins (Gupta, 1999; Dalrymple, 2004). An enormous diversity of palaeovalley sizes, shapes, settings, infills, and potential for hydrocarbon reservoirs and groundwater aquifers predispose them as a "popular" target of study (Zaitlin et al., 1994; Gupta, 1999; Dalrymple, 2004; Breda et al., 2007; Wang et al., 2019; etc.). Although palaeovalleys are commonly occupied by coarse-grained sediments, which are supposed to be less promising for the detection of controlling factors of foreland basin evolution due to poor biostratigraphic evidence, several studies have shown that they can serve as an important source of data for reconstructing the infill history of a basin (Longhitano, 2008; Leszczyński and Nemec, 2015; Gobo et al., 2015).

This paper focuses on a Miocene incised-valley fill near the town of Brno at the distal/cratonward margin of the Western Carpathian Foreland Basin (Moravia, Czech Republic; Fig. 1). Although the valley is still partly detectable in the present landscape, its infill is known mostly from subsurface data. The volumetrically important unit of the valley infill represents coarse clastic deposits known as the Brno sands. These sands constitute an important aquifer of the area and were exploited in the past for a variety of other purposes. This paper provides:

- at a regional level, a sedimentological, architectural and provenance analysis of the Brno sands;
- examination of the factors that determined the location and geometry of the Brno sands within the palaeovalley;
- assessment of the formative conditions of the valley development based on sequence stratigraphic concepts (sediment supply, accommodation space, role of tectonics and

* E-mail: slavek@sci.muni.cz

Received: June 20, 2022; accepted: August 9, 2022; first published online: November 11, 2022

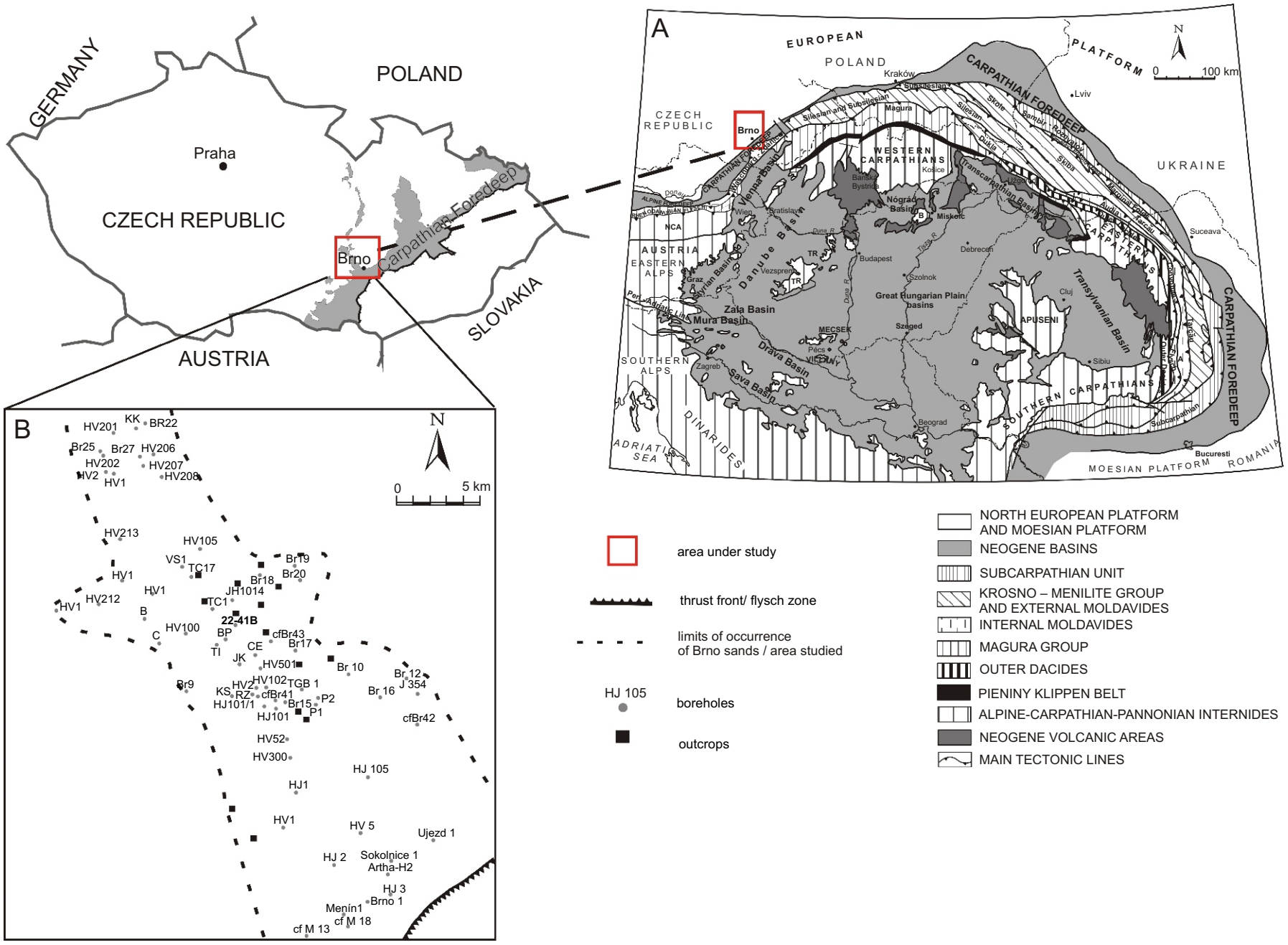

Fig. 1. Geographic location of the area under study

A – position of the study area within the Carpatho-Pannonian region, **B** – detailed position of boreholes and exposures analysed

eustasy) within the evolution of the foreland basin depositional system and basin palaeogeography;
– a contribution to knowledge of the spectrum of foreland entrenched valleys and their infills.

GEOLOGICAL SETTING

A simplified geological map of the broader surroundings of the area under study is shown in Figure 2. The Western Carpathian Foredeep (WCF) constitutes a peripheral foreland basin formed due to the tectonic emplacement and crustal loading of the Alpine-Carpathian Thrust Wedge onto the margin of the Bohemian Massif (Nehyba and Šikula, 2007; Fig. 1A). The stratigraphic range of the sedimentary infill of the WCF is Oligocene/Lower Miocene (Egerian) to Middle Miocene (Upper Badenian) (Brzobohatý and Cicha, 1993; see Fig. 3). The basin continues north into the Polish Carpathian Foredeep Basin (Oszczypko et al., 2006) and south into the North Alpine Foreland Basin (Nehyba and Roetzel, 2000). The lithological and stratigraphical content and basin architecture varies in various parts of the WCF. Local and regional unconformities are developed due to the varying intensity and orientation of flexural loading and spatially different geological and tectonic histories of the basement, along with the polyphase nature of the active basin margin and gradual change of its position (Brzobohatý and Cicha, 1993; Eliáš and Pálenský, 1998; Krzywiec, 2001; Kováč et al., 2003, 2004; Oszczypko et al., 2006; Francírek and Nehyba, 2016; Nehyba, 2018).

The pre-Neogene basement of the segment of the WCF studied is formed by the Precambrian crystalline rocks of the Brno Massif, partly covered by the Devonian to Lower Carboniferous carbonates, Jurassic carbonates and Paleogene deposits of the Nesvačilka trough (Pícha et al., 2006; Kalvoda et al., 2008 – see Fig. 2). The Neogene deposition in the segment of the WCF studied initiated in the Ottnangian/Middle Burdigalian, when the fluvial, lacustrine and brackish Rzehakia Beds accumulated. Marine transgression took place here during the Karpatian/Late Burdigalian. These deposits are preserved only as relics, being eroded during the next depositional cycle of the basin (Brzobohatý and Cicha 1993; Bubík et al., 2005, 2019). Renewed thrusting associated with the Styrian tectonic phase (Early to Middle Miocene) led to a shift of the foreland basin´s depozones generally to the north-west, to basin and foreland reconstruction together with palaeodrainage changes in the backbulge and forebulge zones, and to the start of a new depositional cycle. These deposits are Early Badenian/Langhian and Early Sarravalian in age and are represented by two strongly dominant lithofacies both areally and volumetrically.

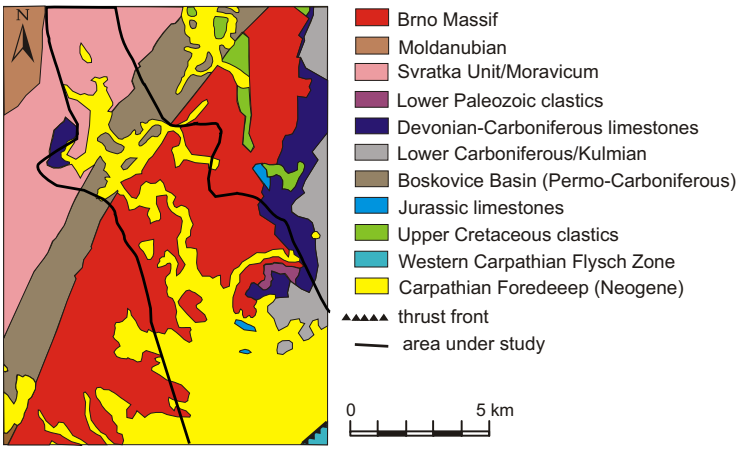

Fig. 2. Simplified geological map of the area under study with position of the study area

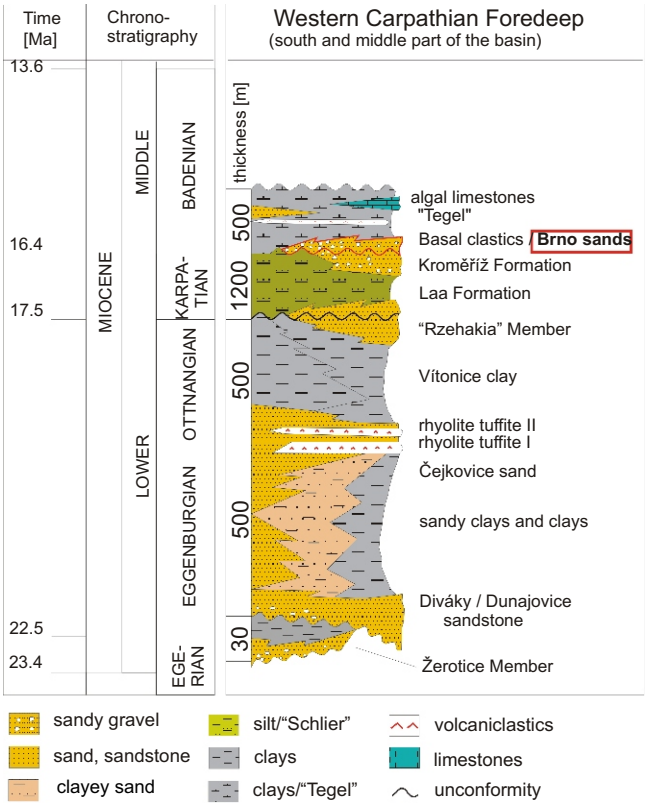

Fig. 3. Generalized stratigraphic scheme of the sedimentary infill of the southern and middle parts of the Western Carpathian Foredeep with position of the Brno sands (modified after Chlupáč et al., 2002; Adámek, 2003)

The first of these lithofacies comprise "basal or marginal coarse clastics", which are known in the segment of the basin studied as the Brno sands (BS). The BS overlie the Brunovistulian Precambrian crystalline/Brno Massif, autochthonous Paleogene deposits of the Nesvačilka trough or older Lower Miocene deposits of the WCF along a highly irregular base. The thickness of BS reaches several dozens of metres in boreholes. The BS are represented by poorly sorted coarse-grained sands, gravelly sands and sandy gravels. The diameter of the coarse clasts generally varies from 1.5 to 10 cm. The largest clasts reach ~50 cm in diameter and the BS are typically described as polymict. Transitions from monomict (only angular granitoid clasts of the Brno Massif) to polymict BS have been recognized at some localities (Krystek, 1974). However, monomict development is missing in most exposures and cores. Krystek (1974) inferred two varieties of BS based on the pebble petrography of various outcrops. The first variety (located generally more to the W or SW) was characterized by a predominance of crystalline rocks + quartz and absence or very low content of carbonates. The second variety (located more to the E or NE) typically had a higher content of carbonates

(Jurassic and Devonian limestones) and lower content of crystalline rocks. The occurrence of several varieties of mudstone (silty clay) intraclasts is typical; these are typically larger than the associated extraclasts. Micropalaeontological studies of the BS (intraclasts and sandy matrix) identified macro- and microfaunal spectra of Early Badenian, Karpatian, Ottnangian and Cretaceous age. Their source is interpreted as a result of redeposition mostly from adjacent sedimentary units and also from the older infill of the WCF itself (Krystek, 1974; Brzobohatý and Cicha, 1993; Bubík and Petrová, 2004; Petrová, 2004; Bubík et al., 2019). The BS were interpreted as beach deposits, shoreface dunes or spits connected with marine transgression (Krystek, 1974). The BS are typically overlain by Lower Badenian grey-green mudstones ("Tegel") or by Quaternary (mostly) fluvial deposits.

The monotonous basinal mudstones ("Tegel") represent the second dominant Lower Badenian lithofacies. Their thickness gradually increases towards the central parts of the basin, where it can reach up to ~600 m. These clays reflect a fully marine depositional environment of the middle to outer shelf with abundant fossils (Tomanová-Petrová and Švábebnická, 2007). A changeable palaeoenvironment, especially as regards sea level fluctuation, and unstable conditions have been documented (Nehyba et al., 2008). Rare and thin interlayers of acidic volcaniclastic deposits are interpreted as distal tephra fallout (Nehyba et al., 1999). These Lower Badenian deposits represent the final stage of deposition within the segment of the WCF studied.

The term BS was used as a local lithostratigraphic unit, being areally distributed along the southwestern margin of the Boskovice Basin and on the Brno Massif (Krystek and Tejkal, 1968; Krystek, 1974). However, the considerable variability in the pebble petrography (see Krystek, 1974), and in sedimentary structures and textures, point to a more complex scenario of depositional processes and palaeogeography within the originally proposed regional extent of the BS. Nehyba et al. (2016) documented that the BS are not developed in the Oslavany sand pit, i.e. a locality which was previously supposed to be their holostratotype (Papp et al., 1978). The term BS is therefore used in this paper in a palaeogeographic sense as a distinct sedimentary unit with a characteristic depositional environment and a regional distribution close to Brno (see Figs. 1 and 3).

METHODS

The study area is located in southeastern Moravia in the close surroundings of the city of Brno. Individual exposures are rare and mostly small. The results are based on the study of 9 exposures (over an altitude range of 225–305 m a.s.l.) and of 98 boreholes. The boreholes have been drilled during the last six decades and mostly only general descriptions of lithology and stratigraphy are available. Preserved cores are rare, discontinuous and mostly small. However, the 22-41B Černá Pole borehole, which was drilled in 2015, provided a completely cored 69 m thick profile of the BS. Locations of both exposures and boreholes are shown in Figure 1B. The altitude of the BS base in boreholes varies between 54 and 281.5 m a.s.l. and the top of BS varies between 86 and 282.5 m a.s.l. A map of the thickness was created in *Surfer 11* software (gridding method) based on borehole data.

Conventional field methods of sedimentological analysis were used, such as detailed logging, evaluation of bedding attitude and palaeocurrent directions, and line drawings of bedding architecture on exposure photomosaics (Collinson and Thompson, 1982; Walker and James, 1992; Tucker, 1995). Lithofacies analysis is based on primary sedimentary structures and textures. Lithofacies were grouped into facies associations, i.e. assemblages of spatially and genetically related facies, which are also the expressions of different sedimentary environments.

Pebble and cobble petrography, shape and roundness were determined both in exposures (clasts >1.6 cm) and in borehole cores (clasts >8 mm). Shape and roundness were estimated mostly visually using the methods of Zingg (1935) and Powers (1982). The maximum pebble/cobble size represents an average of the longest axis (A axis) of the 10 largest extraclasts found in a locality.

Heavy minerals were studied in 10 samples from 4 exposures and borehole 22-41B in the grain size fraction 0.063–0.125 mm, and the translucent heavy mineral assemblages identified were compared with published data (see Krystek, 1984; Bubík et al., 2019). The chemistry of garnet was analysed on 125 grains; the chemistry of rutile was based on data from 29 grains. All grains were randomly chosen. Electron microprobe analysis was done on a *CAMECA SX* electron microprobe analyser (Faculty of Science, Masaryk University, Brno). Measurements were carried out under the following conditions: wave propagation mode, accelerating voltage 15 keV, beam current 20nA, beam size 2 μm. Garnets were checked for internal zoning. Because the grains examined do not show chemical zoning, the chemical composition was examined at single spots located in grain centres.

RESULTS

FACIES ANALYSIS

Lithofacies of the succession studied are summarized in Table 1, and organized into six facies associations (FA). Facies associations are for simplicity labelled with interpretive genetic names, but their descriptions are separated from interpretations in the text. These FA are:

1) topset deposits of the Gilbert-type deltas;
2) foreset deposits of the Gilbert-type deltas;
3) toeset deposits of the Gilbert-type deltas;
4) bottomset deposits of the Gilbert-type deltas;
5) shoal-water delta deposits;
6) offshore marine deposits.

Examples of lithofacies, logs and line drawings, illustrating the distribution of facies associations in exposures and borehole 22-41B, are shown in Figures 4–12.

FA 1 – TOPSET DEPOSITS OF THE GILBERT-TYPE DELTAS

This facies association constitutes a minor proportion of the BS, present only in one exposure. However, some historical photographs (see Fig. 4A–C) of several former exposures provide some additional evidence of FA 1. All occurrences of FA 1 are areally restricted to the NW margins of the area of occurrence of the BS. FA 1 is composed exclusively of medium- to thick-bedded trough-cross stratified sands of facies St. The set thickness reaches several decimetres (Fig. 4D). The total thickness of these sheet-like beds ranges from 0.5 to 3 m. FA 1 is characterized by its stratigraphic position typically overlying foresets (FA 2) and being overlain by open marine deposits (FA 6). The contact between FA 1 and FA 2 is sharp and almost flat with an undulose erosional relief or is broadly concave upwards.

Table 1

Descriptive summary list of lithofacies of the deposits studied deposits distinguished at the exposures studied

Symbol	Description	Interpretation
Gm	Massive/structureless, clast- to matrix- supported fine to coarse pebble gravel, locally lithified. Matrix of coarse to very coarse sand. Pebble clast size usually 1–3 cm, intraclasts are usually larger, up to 6 cm across. Maximum size 15 cm. Non-preferred orientation of pebbles. Polymict gravel, rounding of pebbles greatly varies – subangular and subrounded pebbles dominate. Tabular to lenticular beds with sharp concave bases and sharp inclined flat slightly irregular tops. Bed thickness varies from 0.2 to 1.5 m.	Deposits of cohesionless debris flows (Nemec, 1990; Gobo et al., 2015)
Go	Layers of gravel formed either by isolated clasts or clasts are in contact with one another forming irregular gravel clusters/lenses usually a few clasts thick (locally reaching up to 20 or 50 cm in thickness), clast-supported or openwork or forming irregular a few to single clast-thick clast clusters/pebble stringers with varied lateral continuity. Locally terminating abruptly within a few meters, sometimes laterally persistent over an entire exposure. The clasts are mostly pebble-sized, cobbles are present only in subordinate amounts and boulders are exceptional (1.2 m across). Intraclasts are typically larger than extraclasts. Clasts are angular to rounded. Interstices between the gravel clasts are filled with sand matrix. Clasts can be variably oriented, however, A-axis of outsized clasts is oriented often parallel to stratification, less commonly perpendicular and imbricated. Typically form interbeds within beds of Gsa. Sharp slightly undulose base, irregular tops of beds.	Debris fall deposits (Nemec, 1990; Sohn et al., 1995) or outrunning clasts from cohesionless debris flows (Sohn et al., 1997)
Gsa	Thin- to medium-thick beds of coarse to very coarse sand to fine or medium pebble gravel alternate with thin beds of fine to medium coarse sand. Frequent grain size fluctuations on a thickness scale of 1 to 3 cm. Planar parallel stratification well to faintly developed. Inclination of stratification strongly varies (between 5 and 30°). Scattered isolated pebbles with A axis of elongated pebbles mostly oriented parallel to stratification. Rare and scattered shell debris (molluscs). Mostly tabular beds with lateral continuity over an entire exposure or pinching out within several metres. Sharp planar or broadly concave tops and bases of beds.	Traction deposition from high-density turbidity currents (Lowe, 1982) or deposition from diluted cohensionless debris flows (Sohn et al., 1997), sustained and fluctuating flows (Plink-Björklund and Ronnert, 1999).
Gsx	Thick- to medium-thick beds of clast- to matrix-supported fine to coarse pebble gravel (matrix of coarse to very coarse sand) alternate with thin beds of medium to coarse sand. Planar cross-stratification, tangential or sigmoidal in shape. Scattered isolated pebbles and cobbles (exceptional boulders of intraclasts up to 40 cm across) with A axis of elongated clasts mostly oriented parallel to stratification. Roughly tabular to wedge shape of beds. Bed thickness ~2 m. Sharp slightly undulose, inclined bases (10–20°), sharp inclined tops.	Tractional deposits filling small-scale channels cut within deltaic foresets
Gg	Matrix (medium to coarse sand) supported fine to medium pebble gravel, massive, normally graded at the base passing upwards into faintly planar parallel-stratified. Tabular shape of beds. Bed thickness 10 to 60 cm. Sharp erosive planar or broadly convex down bases, rarely with scattered small pebbles up to 6 mm across (long axis parallel with the base). Sharp flat tops.	Deposition from high-density turbidity currents (*sensu* Lowe, 1982); rapid deposition
St	Medium grained sand, poorly sorted due to admixture of grains of very coarse sand to granules up to 0.3 cm in diameter. Locally rich irregular intraclasts of mudstone up to 1 cm in diameter. Trough cross-stratification with fining upwards trend due to reduction in content of granules. Irregular shape of beds. Sharp broadly partly convex down bases inclined (inclination generally in the similar direction as the dip of underlying foresets). Flat sharp tops. Set thickness 10–25 cm. Bed thickness up to 2 m. Bioturbation absent.	Migration of 3D bedforms – dunes (Bridge, 2003)
Sxu	Solitary, discontinuous trough-shaped scours filled with cross-stratified poorly sorted coarse to medium sands or gravelly sands showing an upslope (relative to the bedding planes of foresets) angular cross-stratification (dip between 10 to 30°). Scours reveal a convex down base and generally flat top. They are 10 to 40 cm deep and pinch out both up-dip and down-dip.	Backsets formed due to hydraulic jump on a steep delta slope (Nemec, 1990, Massari, 1996; Breda et al., 2007); scour infill at the toeset
Sl	Fine, fine to medium or coarse sand, relatively well-sorted, plane parallel stratified, commonly inclined, rarely slightly undulose. Alternation of laminae of slightly finer and coarser grains. Micaceous. Rare outsized clasts (intraclasts up to 7 mm across). Bed thickness 10 to 50 cm, amalgamated beds up to 4 m. Tabular shape of beds, sharp planar bases and tops of beds.	Tractional deposition by hyperpycnal flow (low-density turbidity currents *sensu* Lowe, 1982)
Sm	Fine, medium, coarse to very coarse-grained sand, structureless/massive. Rare occurrence of shell fragments. Relatively poorly sorted, micaceous. Bed thickness 10 to 40 cm. Sharp, relative flat inclined bases and tops of the beds. Commonly alternating with facies Sl, interbeds within facies Gsa.	Coarse-grained variety – cohesionless debris flow deposits. Fine-grained variety – rapid deposition from suspension (Postma et al., 1988; Mulder and Alexander, 2001)
Sg	Coarse to very coarse sand with rare scattered intraclasts, massive, normal grading, gradually passing upwards into well-sorted fine, fine to medium sand with planar parallel-stratification. Bed thickness 10–65 cm. Very rare transition of inverse to normal grading along the basal portion. Rare occurrence of shell debris. Tabular beds with sharp erosive planar or slightly irregular bases and sharp flat tops.	Deposits of high- to low-density turbidity currents (*sensu* Lowe, 1982). Surge-type turbidity currents (Eilertsen et al., 2011)
Sc	Fine to very fine sand, well-sorted, planar parallel lamination. Common intraclasts (up to 1 cm in diameter) of coal or thin coal interlaminae. Bed thickness 5 to 37 cm. Relatively sharp flat bases and tops of the beds.	Plane bed macroforms deposition from suspension and traction in shallow water (Smith, 1974; Cheel and Middleton, 1986; Bridge, 1993)
Mm	Massive mudstone (clayey silt/silty clay), forming either thick beds or irregular interbeds (mostly within thick beds of facies Sl) max. 5 cm thick. Relatively well-sorted. Rare plastic deformation or content of marine shells or shell debris (molluscs). Sharp flat tops and bases of beds. Bioturbation slight or absent.	Deposits of fallout from open marine suspension and river-derived hypopycnal suspension plumes (Nemec, 1995)
Mh	Light grey mudstone (clayey silt). Rhythmic alternation of laminae to very thin beds (up to 2 cm in thickness) of silty clay and clayey silt. Variations in colour, content of fossil plant detritus, fossil pellets, shell debris. Bioturbation slight or absent. Thick to very thick tabular beds.	Deposition by fallout from suspension below wave base, fluctuations in sediment supply, deposition rate, oxygen content (seasonal or climatic control ?)
C	Dark grey to black grey silty mudstone very rich in coalified organic matter – coaly mudstone. Planar parallel lamination. Lamina to very thin bed thick 1.5 cm. Both tops and bases of the beds are sharp, flat to only slightly undulose.	Suspension settling in a low-energy, poorly-oxygenated, environment. Abundant organic supply

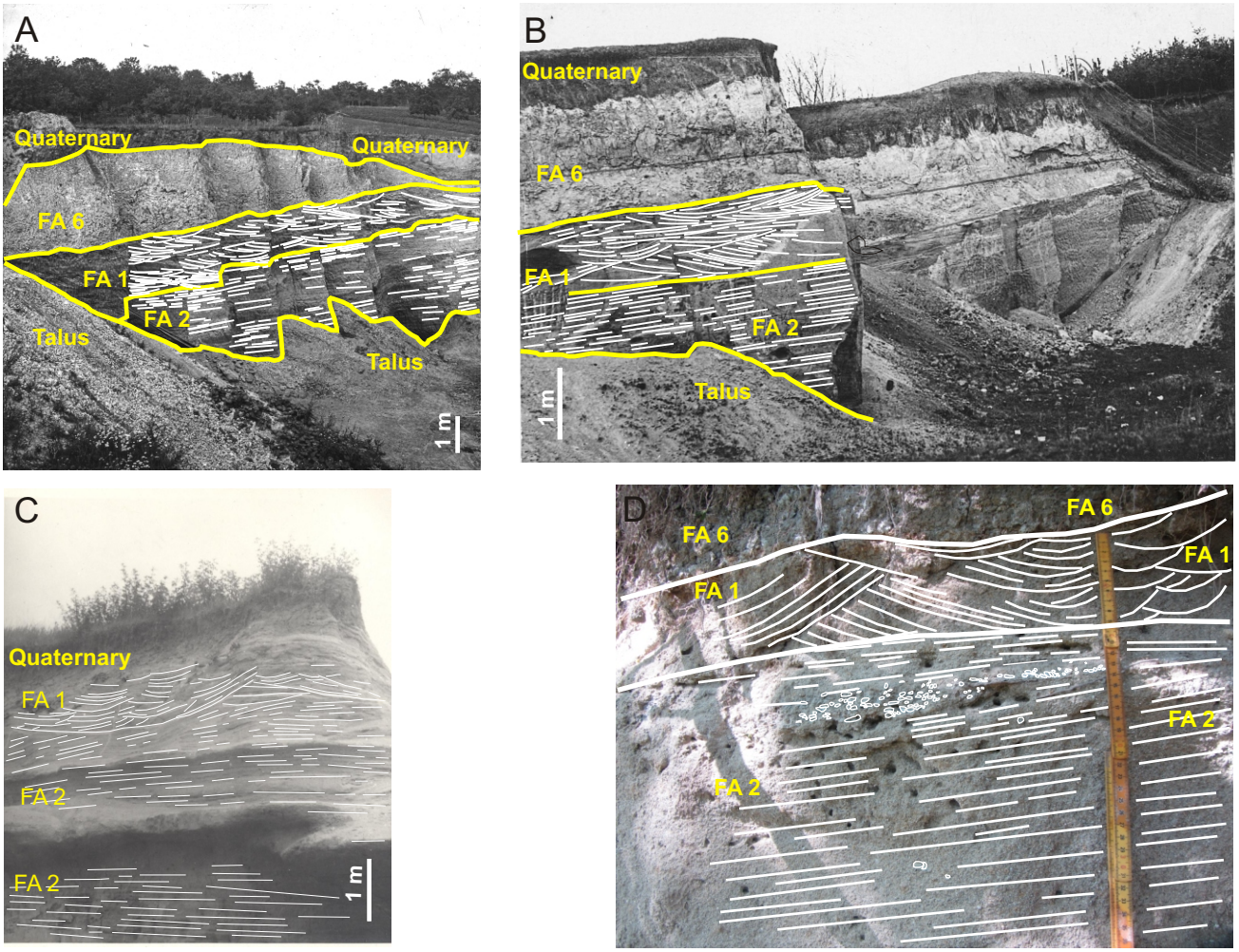

Fig. 4. Field photos of topset deposits (FA 1)

A – sandpit near Brno-Královo Pole without closer location (from Březina et al., 2019); **B** – sandpit under waterworks near Soběšice (from Březina et al., 2019), described thickness of FA 2 of ~4 m, thickness of FA 1 of ~3 m, thickness of FA 6 of ~2 m and Quaternary deposits with thickness of ~4 m; **C** – sandpit near Brno-Obřany (from Březina et al., 2019), total thickness of Brno sands of ~12 m; **D** – field photo with topset (SF 1) overlying foreset bed (SF 2) and being overlain by offshore mudstones (FA 6); A–C – historical photographs from the presently unexposed sandpits showing the vertical succession of the Brno sands: foreset (FA 2 – bottom of the photographs) to the topset (FA 1 – middle of the photograph to offshore mudstones/Tegel (FA 6) and Quaternary deposits (top of the photograph), note the cross-stratification facies composing the topset; authors of photos unknown; scale – 1 m

This base of FA 1 is also typically gently inclined "seawards" (i.e. generally in the foreset dip direction). The top of FA 1 is also sharp, generally flat or broadly undulose.

Interpretation: the stratigraphic position allows interpretation of the FA 1 deposits as the topset, i.e. bedload deposits forming 3D dunes on the distributary plain of a Gilbert-type delta or deltas. Channelized beds (Fig. 4C) are generally characteristic of a fluvial-dominated topset and represent the prolongation of fluvial channels within the delta plain that supplies the deltaic systems. Deposition of the river bedload causes vertical accretion (Bridge, 2003). Trough cross-stratification, a fining-upwards trend and mudstone chips suggest broad channelized flow transport in a highly dynamic river system, which was characterized by shallow, unstable and low-sinuosity channels and a high sediment discharge, typical of braided river systems (Miall, 1996). The mudstone chips may signal erosion of floodplain fines. The general fining and thinning upward trend of the FA 1 succession indicates waning flow and filling of the available space connected with the final stages of fluvial deposition, progressive lowering of the stream gradient and decreased flow depth. Such a situation might reflect marine flooding of the fluvial plain.

The sharp and erosive contact between topset/FA 1 and foreset/FA 2 (see Fig. 4) reveals an oblique delta-brink geometry (Gobo et al., 2015). The contact of the basinal clays (FA 6) and topset (FA 1) is attested as the topset breakpoint path (Backert et al., 2010). Such a topset breakpoint path is a key stratal surface, which records a significant landward facies shift and a rapid increase in accommodation/sediment supply ratio.

Missing evidence of topsets at the majority of exposures is explained by the rapid drowning of the delta by the next transgression with a rapid upslope shift of the facies belt, and could also point to a narrow deltaic plain typical of high-relief basement settings (Nemec, 1990). Topset absence is commonly explained by erosion due to base-level-fall (Budai et al., 2021). The possibility that all available logs were measured basinwards of the point of maximum delta brink progradation is less probable. The strong reduction in FA 1 thickness (with respect

to the underlying FA 2 foreset) and its preservation only in marginal/landward terminal parts of the generally prograding Gilbert-type delta depositional system may be evidence of more complex palaeogeographical and stratigraphic factors recorded within the BS succession.

FA 2 – FORESET DEPOSITS OF THE GILBERT-TYPE DELTAS

This facies association consists of inclined (10–30°) clinostratified sands, gravelly sands and gravels. They are laterally (Fig. 5A) and vertically (Fig. 5B) stacked up to form bodies several tens of metres thick, which are laterally persistent for hundreds of metres. They stratigraphically overlie mostly the pre-Neogene basement (Fig. 5C), less commonly toeset deposits (FA 3), and are typically overlain by open marine deposits (FA 6) (Fig. 5D), rarely by topset (FA 1) (Fig. 4) or by shoal-water delta (FA 5) deposits. The FA 2 deposits consist of 10 facies (Gsa, Go, Sl, Sg, Mm, Gm, Gg, Sm, Gsx and Sxu) and constitute the main portion of the BS succession.

Thin to moderately thick beds of coarse to very coarse sand to fine pebble gravel alternating with very thin to thin beds of medium to fine sand of facies Gsa represent the predominant portion of FA 2 in most exposures (Fig. 6A–D). The most common feature is diffuse planar, crude to very regular stratification, in most cases parallel (or at low angles) to the master bedding. The stratification is from <1 cm (i.e. laminae) to 15 cm thick. Amalgamated beds of Gsa are several metres thick. Shell debris (molluscs) is rare and scattered.

Interbeds of outsized clasts (lithofacies Go) are recognized in most exposures, typically within thick Gsa beds. Clasts occur in isolation, or form thick clusters/pockets a few clasts thick, or they are aligned in more or less continuous rows (Fig. 6D–H). They can locally form lenticular beds of clast-supported to openwork cobble to pebble gravels which are up 0.5 m thick. The a-axis of outsized clasts is oriented mostly parallel to stratification, less commonly perpendicularly and imbricated. Clasts are mostly angular to subangular and of pebble size (up to 5 cm across) mudstone intraclasts are typically larger. However, some mudstone clasts can reach 0.5 m and extraclasts 15 cm across. These cobbles and boulders are present only in subordinate amounts.

The Gsa lithofacies typically alternates with thin- to medium-thick tabular beds of fine- to medium- or coarse-grained sand with plane parallel stratification of facies Sl. Alternation of laminae with grain size fluctuations is characteristic for Sl lithofacies (Fig. 7A, B).

Significantly less common is the occurrence of thin- to medium-thick beds of coarse to medium, medium- to fine-grained massive sand, with rare occurrence of shell fragments of lithofacies Sm (Fig. 7C).

The interbeds of lithofacies Sg formed by massive sands with normal distributional grading, gradually passing upward into well sorted fine, fine to medium sand with planar parallel-stratification

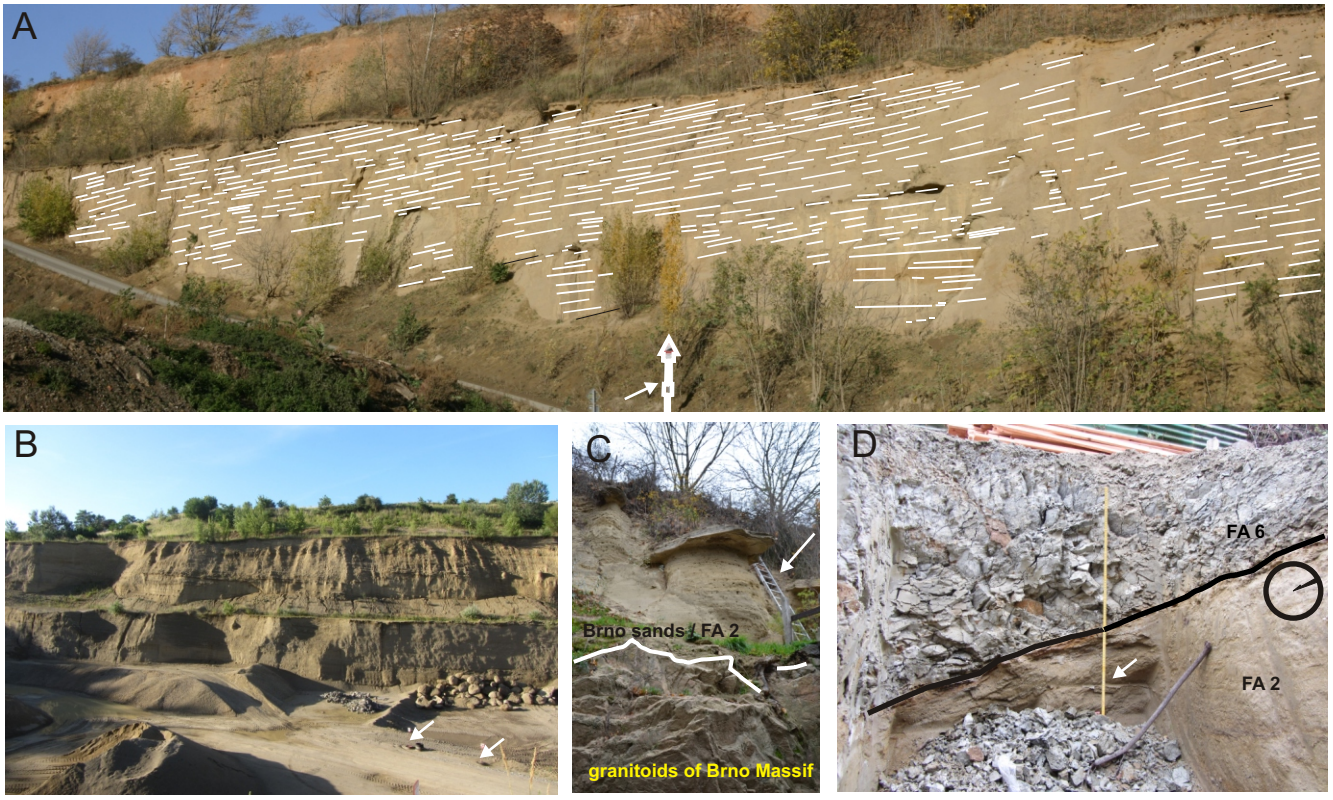

Fig. 5. Photos of the exposed section studied

A – western part of the Černovice exposure with laterally stacked foreset deposits, white arrows point to traffic sign (height 3.2 m); **B** – vertically stacked foreset beds on the exposed section of Staré Černovice, white arrows point to traffic signs (height 2.3 m); **C** – basal contact of foreset beds with crystalline basement of the Brno Massif (white line), white arrow points to a ladder (height 2.5 m); **D** – foreset beds (FA 2) sharply overlain by open marine deposits (FA 6), white arrow points to 1 m scale; inset rose diagram reveals transport direction towards the NW

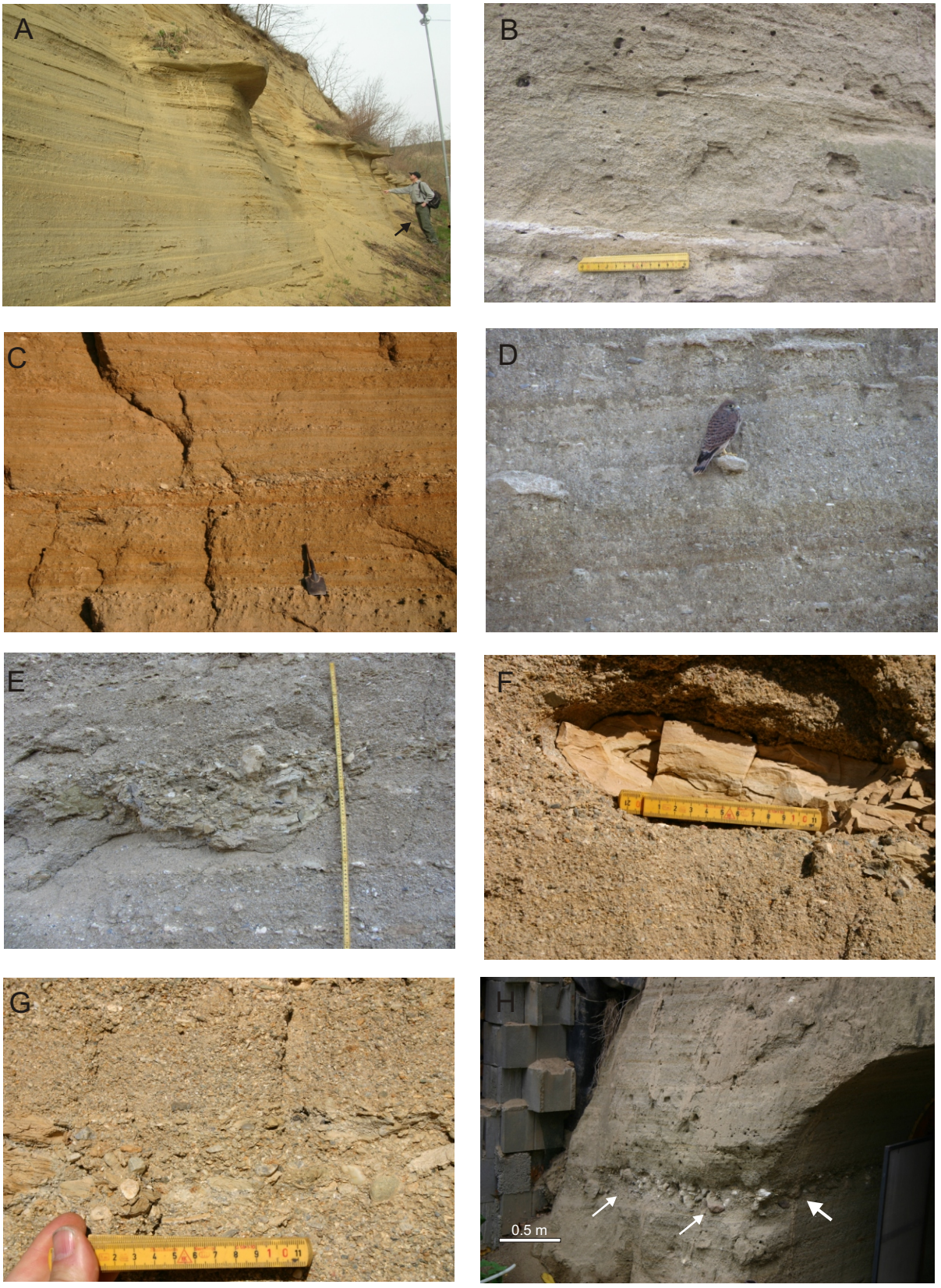

Fig. 6. Selected examples of lithofacies of facies association 2/foreset

A – thick amalgamated beds of facies Gsa, a person marked by black arrow for scale; **B** – well-developed inclined stratification of facies Gsa; **C** – interbeds of lithofacies Go within beds of lithofacies Gsa; **D** – scattered outsized extraclasts (Go) within lithofacies Gsa, kestrel for scale; **E** – cluster of outsized clasts (both extra- and intraclasts) of lithofacies Go; **F** – large intraclasts in the early stages of disintegration scattered within beds of lithofacies Gsa; **G** – detail of clast-supported gravels of lithofacies Go; **H** – lithofacies Go aligned as an almost continuous row of clast-supported extraclasts with imbrication

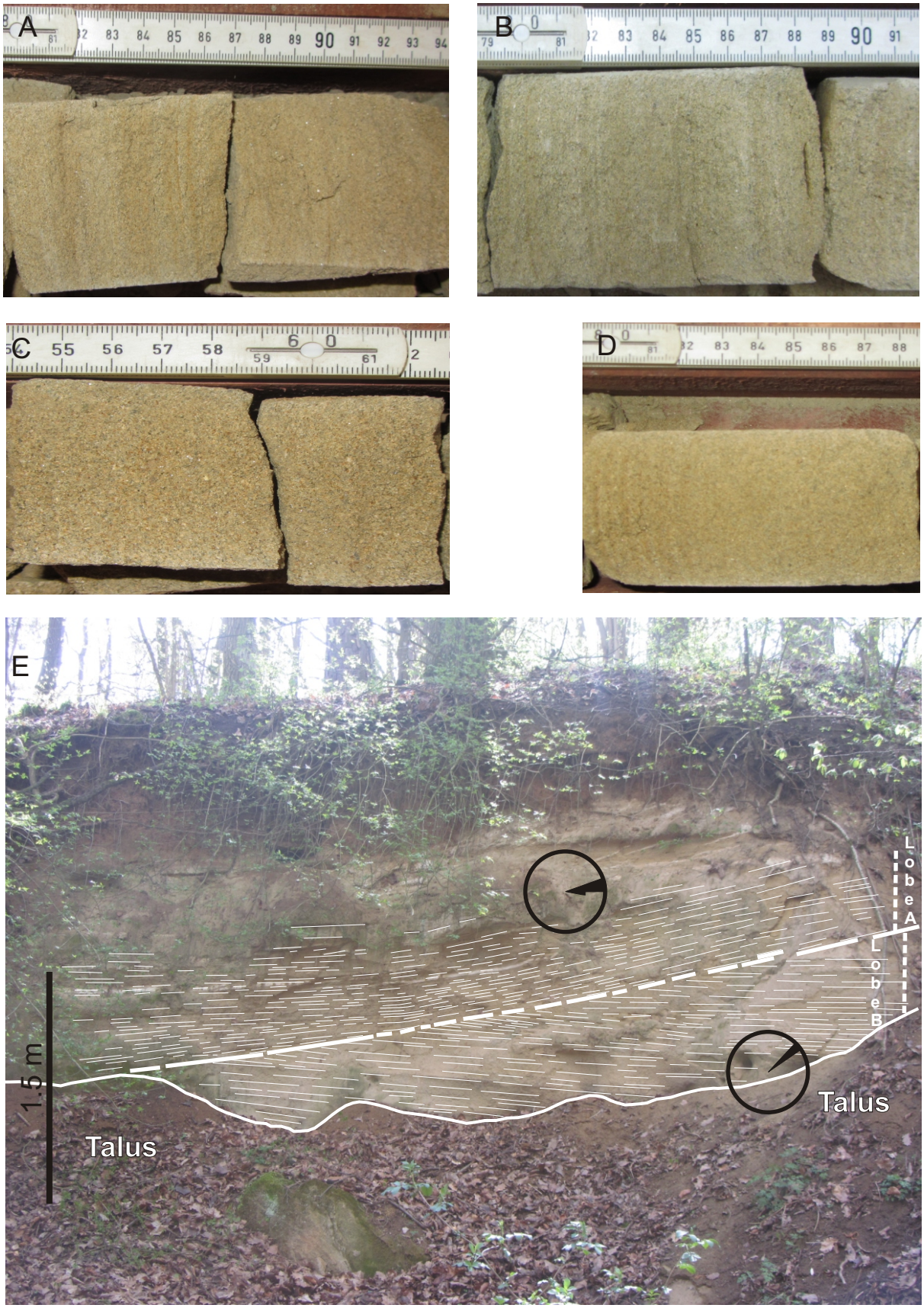

Fig. 7. Selected examples of lithofacies and field photo of facies association 2

A – lithofacies Sl, **B** – lithofacies Sl, **C** – lithofacies Sm, **D** – lithofacies Sg, **E** – internal truncation of foreset beds separating two foreset lobes/units with a little variation in the orientation of the foreset dip (as show by inset rose diagrams)

are rare (Fig. 7D). Similarly rare are occurrences of very thin beds of massive mudstone of lithofacies Mm.

Very thick beds of unorganized massive, matrix supported pebble to cobble gravel of lithofacies Gm are exceptionally observed in outcrops; however, they are more common in borehole cores. Gravel is poorly sorted and contains subrounded to subangular extraclasts/pebbles (mostly ~2–3 cm), outsized mudstone intraclasts (up to 15 cm across), which are mostly dispersed in the lower portion of the bed. The matrix is formed by coarse to very coarse gravelly sand. The outcropped bed of facies Gm reveals wedge shape tapering upslope due to an erosive sharp, relatively steep (dipping up to 55° downslope relative to foreset bedding) concave basal surface and a sharp flat slightly inclined upper boundary. The thickness of the bed reaches 2 m; however, the deposits are pinching out laterally at an outcrop scale (distance of several metres). The Gm bed is sandwiched within thicker packets of stratified Gsa and Sl deposits. Different dips and strikes of the large scale stratification are observed for the underlying and overlying packet (Fig. 8A, B).

Clinostratified beds commonly reveal a regular, sheet-like geometry laterally persistent over an entire exposure. Detailed observation of a bed with apparent lateral continuity reveals that its individual foreset beds are in reality discontinuous, wedge-shaped, and gradually pinch out in the down-slope direction towards the toes of the foresets. This suggests a tongue-like geometry in general. Foresets are locally truncated by concave-up or planar surfaces (Figs. 7E and 9A).

The foreset dip orientations vary significantly between individual exposures, as foreset beds dip westwards, south-westwards, southwards, south-eastwards and north-eastwards. However, the orientation is relatively stable within individual exposures. A flattening tangentially downdip to 5 to 10° is recognized in some cases (see Fig. 9B).

Along the foresets, relatively thin (up to 2.5 m thick) units occur, characterized by sigmoidal geometry and internal cross-stratification inclined downslope (i.e. generally in the similar direction to the foreset) described as lithofacies Gsx (Figs. 9A, C and 10A, B). These are represented by alternating cm- to dm-thick convex-down sets of coarse to very coarse sand with an increase in the foreset dip angle towards the base (~30°). These units can be followed for several tens of metres. They reveal sharp, erosional, concave-up lower boundaries blanketed by several cm-thick pebble cobble gravel beds (Go), markedly enriched in mudstone intraclasts (up to 0.4 m across), which are significantly larger than the intraclasts scattered within lithofacies Gsa. The gravels are clast-supported to openwork, structureless, with subangular to subrounded clasts, commonly laterally aligned along the bed bases. The matrix is formed of very coarse sand to fine pebble gravel (Fig. 10C). The convex-up upper boundary is diffuse and the sigmoidal unit pinches out within sheet-like foresets of lithofacies Gsa (see Figs. 9A and 10A, B).

Isolated scours filled by medium- to coarse-grained sands with scattered pebbles, of facies Sxu, are recognized rarely. Cross-stratification dipping upslope (~20–30°) relative to foreset bedding (formed by Gsa lithofacies) is typical. Spoon-shaped scours are ~0.5 m deep and can be followed over a distance of a few metres (Fig. 11A).

The distribution of individual lithofacies of FA 2 vary between individual exposures. The relatively coarser-grained lithofacies Gsa strongly dominates (forming 46 to 90%), accompanied by lithofacies Go, Sl, Sm, Gsx, in most exposures. How-

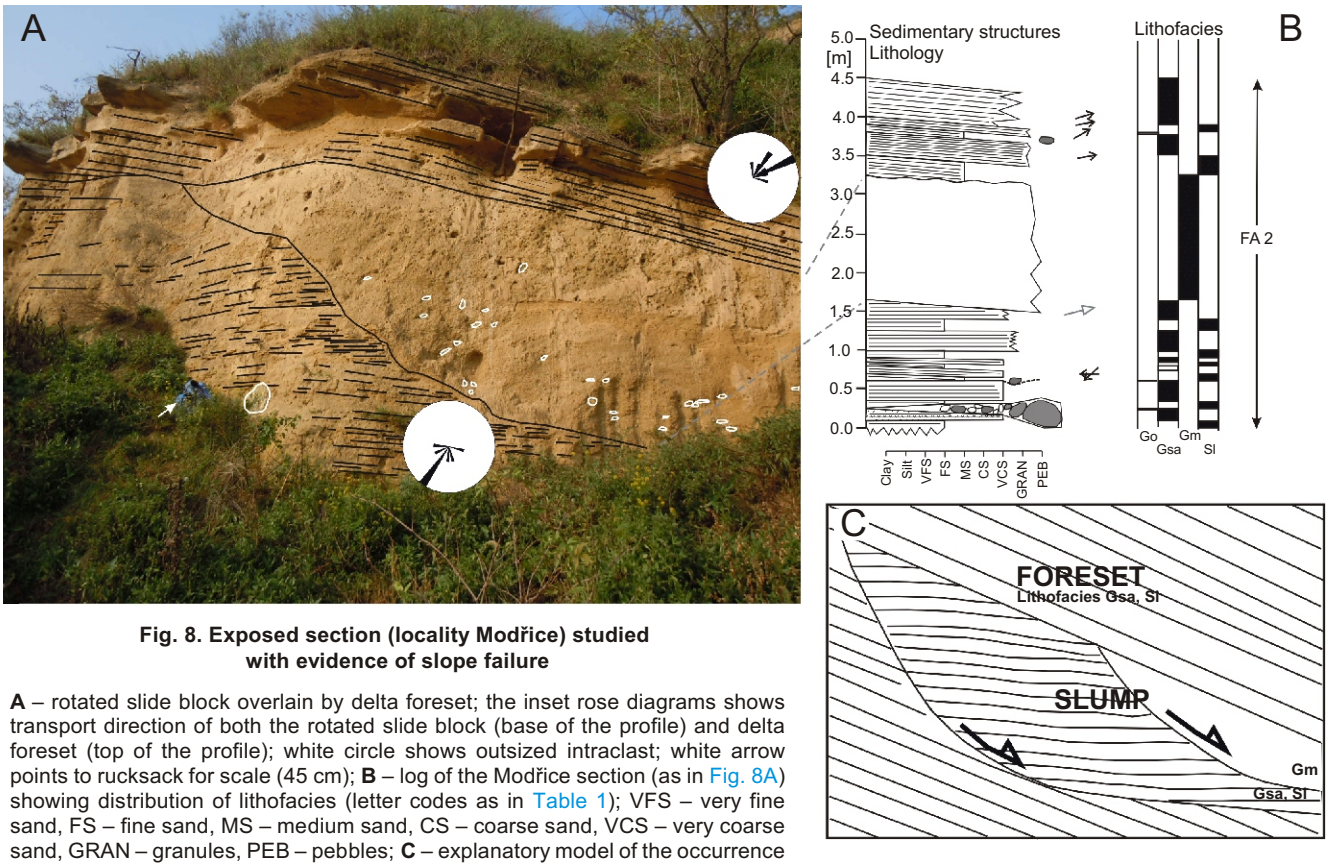

Fig. 8. Exposed section (locality Modřice) studied with evidence of slope failure

A – rotated slide block overlain by delta foreset; the inset rose diagrams shows transport direction of both the rotated slide block (base of the profile) and delta foreset (top of the profile); white circle shows outsized intraclast; white arrow points to rucksack for scale (45 cm); **B** – log of the Modřice section (as in Fig. 8A) showing distribution of lithofacies (letter codes as in Table 1); VFS – very fine sand, FS – fine sand, MS – medium sand, CS – coarse sand, VCS – very coarse sand, GRAN – granules, PEB – pebbles; **C** – explanatory model of the occurrence of the rotated slide block at the exposure

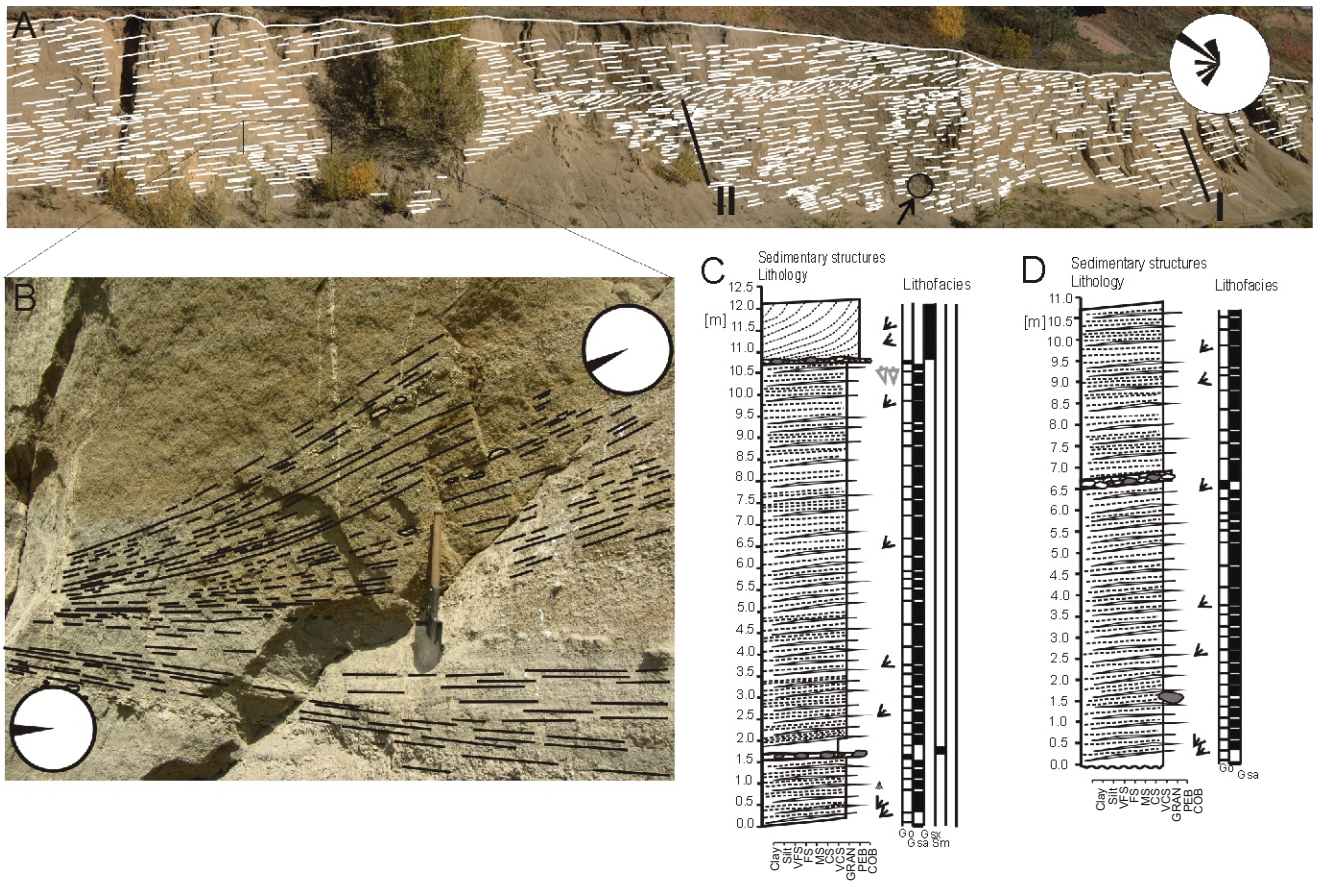

Fig. 9. Field photos and logs of the studied succession

A – locality Černovice upper section showing the foreset organization with changes of the delta building; the inset rose diagram show palaeotransport direction measured from foreset bedding; location of the logs I and II, outsized intraclast (1.2 m across) circled and marked by black arrow; black rectangle shows approximate position of Figure 9B; **B** – flattening of foreset bedding tangentially downdip; **C** – sedimentological log II; **D** – sedimentological log I (letter codes as in Table 1); COB – cobble, for other explanations see Figure 8

ever, in a few a finer-grained facies such as Sl, Sg dominates, in places accompanied by thinner beds of lithofacies Gsa and Go.

FA 2 is 64 m thick in borehole 22-41B. The succession of FA 2 can be here subdivided into two sub-associations which alternate: mostly thinner-bedded sand-dominated FA 2.1 and relatively thicker-bedded gravelly FA 2.2.

FA 2.1 is characterized by strong (>70%) dominance of medium to very thick-bedded (up to 6.8 m) fine- to medium- or coarse-grained sand with plane parallel stratification of facies Sl. Less frequently (~17%), medium- to thick-bedded, fine-, medium-, coarse- to very coarse-grained, massive sands of facies Sm and planar parallel-stratified, coarse to very coarse gravelly sands of facies Gsa were recognized. Isolated extraclasts up to 1 cm in diameter and rare intraclasts of grey mudstone up to 3 cm are followed by facies Gsa, with common a(p) prolonged clast fabric. Thin- to medium-bedded massive, clast-supported fine to coarse pebble gravels of facies Gm or massive sands with normal distributional grading, gradually passing upwards into well-sorted fine, fine to medium sand with planar parallel-stratification of facies Sg are significantly less common (2.3–4.8%). The occurrence of irregular, very thin interbeds of facies Mm within thick beds of facies Sl is exceptional. The thickness of FA 2.1 is 8.7 and 22.1 m.

FA 2.2 consists volumetrically dominantly (52.5–68.8%) of thick to very thick (up to 6.1 m thick) beds of coarse to very coarse planar parallel-stratified sand with scattered granules to small pebbles or sandy gravel of facies Gsa. The occurrence of medium- to very thick-bedded massive clast-supported fine to coarse gravel of facies Gm greatly varies (0.7–29%), similarly to the occurrence of medium- to very thick-bedded normally graded fine pebble gravel of facies Gg (0–15.3%). Similarly (but in contrast to the occurrence of facies Gm and Gg) the occurrence of medium- to very thick-bedded fine, medium- to coarse-grained planar parallel-stratified sands of facies Sl (1.1–29.4%) is highly variable. Less common and thinner are thin to medium thick beds massive sands (facies Sm), normal graded, planar parallel-stratified sands (facies Sg), and massive mudstones (facies Mm) forming between 1.1 and 3.2% of the FA 2.2. succession. The thickness of FA 2.2 was 13.2 and 16.6 m.

Interpretation: high-angle tangential bedding is consistent with descriptions of Gilbert-type delta foresets with gravity-driven sediment transport and deposition (e.g., Postma and Cruickshank, 1988; Nemec, 1990; Sohn et al., 1997; Longhitano, 2008; Martini et al., 2017). A variety of depositional processes occurred along the foresets.

Beds of facies Gsa and Sl are interpreted as deposits of low-density turbidity flows. Deposits of facies Sg represent high- to low-density turbidity currents (*sensu* Lowe, 1982). Facies Gg is interpreted as the deposit of high-density turbidity currents. Normal grading and fining of individual beds reflect deposition from waning surge-like currents (A and B-divisions of Bouma, 1962). Fine-grained varieties of facies Sm are interpreted as deposits of high-density turbidity currents by gradual aggradation (S3; cf. Lowe, 1982) or rapid deposition from sus-

Fig. 10. Delta foreset facies association at the Černovice locality with line drawings

A – two vertically stacked units/delta lobes with a small sigmoidal microdelta in the centre of the section; white rectangle shows approximate position of Figure 10B; **B** – detailed view of the sigmoidal cross-stratification of facies Gsx filling the main part of the microdelta; **C** – contact of the microdelta basal facies Go and underlying facies Gsa

pension. Coarse-grained varieties of facies Sm are interpreted as cohesionless sandy debris flows (Mulder and Alexander, 2001). Beds of Gm facies are interpreted as non-tractional deposits of cohesionless debris flows (Lowe, 1982; Nemec et al., 1984; Gobo et al., 2015). Facies Go is interpreted as debris fall deposits (Nemec, 1990) and suggests a steep slope upon which sediments can gain high downslope mobility, overcoming the frictional resistance of the substrate (Kim et al., 1995). Some clast-supported open-work gravel may represent tractional bedforms (Russell, 2007). Massive mudstones of facies Mm are interpreted as either large intraclasts (in borehole cores) or as erosional relics of "background" dilute suspension plume deposits accompanying the turbidity currents (very thin beds in exposures). Exceptional Sxu deposits are interpreted as backsets filling slope chute-fills formed by low-density turbidity currents subject to hydraulic jumps (Massari and Parea, 1990; Breda et al., 2009).

Slope failure is documented rarely in exposures (Fig. 8). Gravity collapse of the steep foresets led to the formation of foreset truncations separating individual clinoforms/delta lobes. A sharp steep concave-up basal surface truncating the foreset is interpreted as a scar (Kim et al., 1995) separating a slump bed, an interpretation supported by the lack of internal organization, poor sorting, wedge shape and erosive contact with underlying beds. These deposits differ from foreset beds, which are usually highly organized and display well-developed stratification and lack wedge-shaped geometry. Lithofacies Gm is a product of mass flow processes typically located in upper foresets and which are supported by a high rate of sediment delivery (Breda et al., 2007). The occurrence of debris flows corresponds with the combination of high-bedload events of fluvial discharge to the delta front, or slope instability events (Nemec, 1990).

Common debris fall deposits indicate high-gradient delta foreset slopes (e.g., Nemec, 1990; Sohn et al., 1997), which corresponds to the recognized high-angle bed dip (25–30°) and the occurrence of internal erosion surfaces, indicative of intense sediment sloughing by means of chutes and large-scale slope failures (e.g., Nemec et al., 1999). The foreset slopes are locally dissected by incised small-scale downslope-running chute/channels produced due to the steep gradient of the delta slope together with the energy of gravity currents.

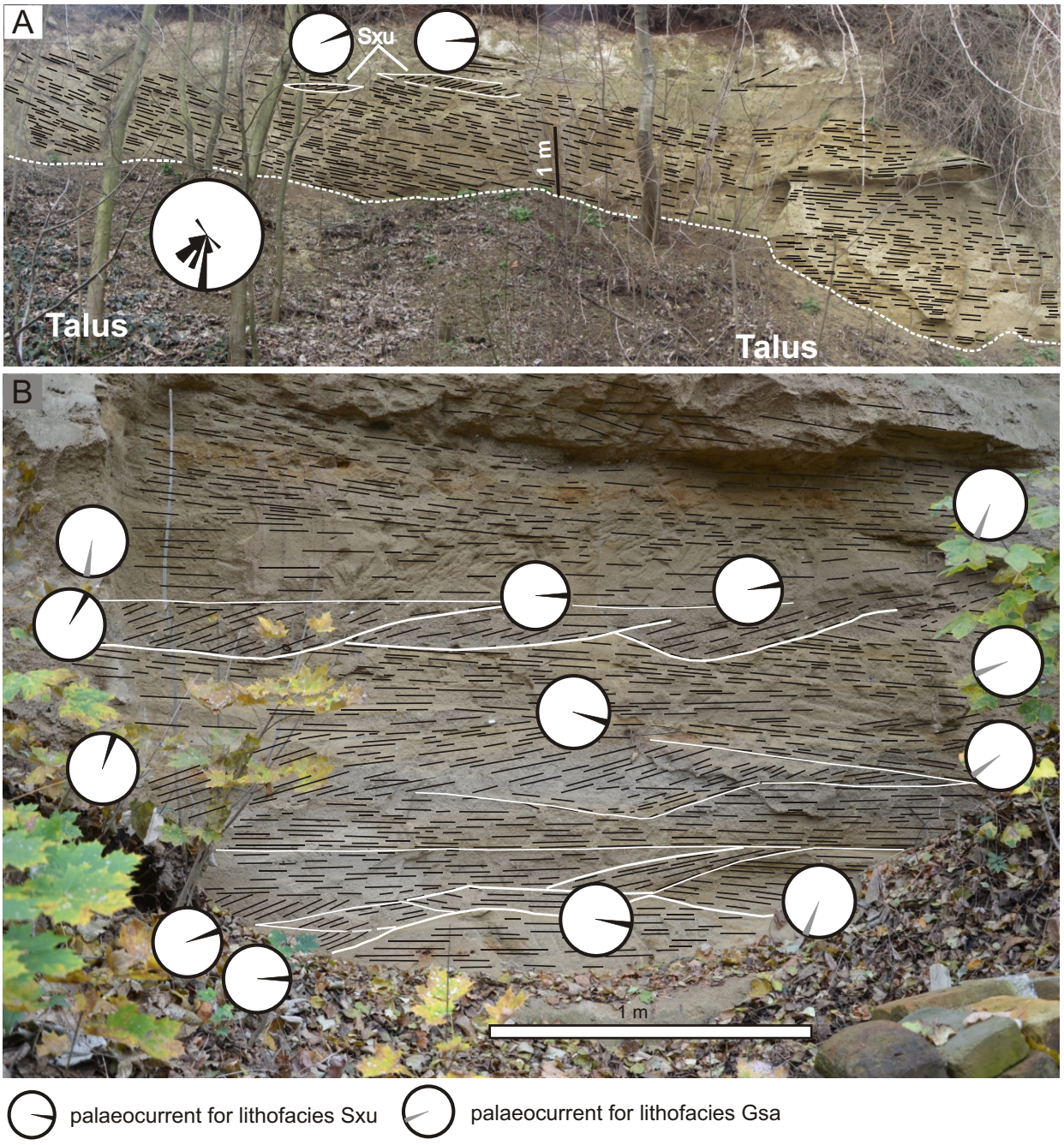

Fig. 11. Typical features of the Gilbert-type delta deposits studied

A – scattered backsets (facies Sxu) within foreset beds. The scour-based backsets (dip 20–30°) are scattered within the bedding (dip ranges from 5 to 10°). The inset rose diagrams show transport direction of both foreset bedding and backset infill. The exposure laterally transits to toeset beds (see Fig. 10B); **B** – field detail of delta toeset faces association. Toeset deposits of lithofacies Sxu (filling scoop-shaped scours) interbedded with lithofacies Gsa continuing from adjacent foreset (transition to foreset to the right – see Fig. 10A). Notice the reduced dip angle of the foreset (compare to Fig. 10A). The inset rose diagrams show transport directions of both foreset and toeset (generally contradictory directions of inclination of Sxu and Gsa)

Their typical shape is controlled by sharp broad concave-up basal scour surfaces and planar almost flat tops. They are filled with sigmoidal beds of Gsx lithofacies overlying basal Go lithofacies. The sigmoidal pattern and relatively enriched content of pebbles indicate a high rate of sediment supply and rapid filling of chutes. The progradation of small "point-bar type" sigmoids (Longhitano, 2008), "microdeltas" (Hwang and Chough, 1990) or channelized and lobate gravelstones and sandstones (Hwang et al., 1995) were interpreted similarly. Chutes/swales might merge downslope to form channels with splays or lobes (Kim and Chough, 2000).

The overall tongue geometry with the wedge shape of the beds suggests emplacement by a series of closely spaced, small volume flows moving over short distances, or by surging behaviour (Sohn et al., 1997). This could be connected with flows with fluctuating bedload discharge. These discharge fluctuations may be indirectly reflected also by variations in the content and size of the intraclasts. Relatively subtle stacked clino-

forms separated by erosional surfaces recognized in some exposures may signal the proximal part of the delta (Colella, 1988; Breda et al., 2007).

The foreset beds show variations in thickness, grain size and lithofacies distribution at individual exposures and/or the borehole succession i.e. both laterally down- and across-transport directions and in time. These variations within the sedimentary succession can be used for evaluation of the proximal to distal evolution of foresets.

Deposits of FA 2.1 are interpreted as sandy foresets of a Gilbert-type delta with a strong dominance of low-density turbidity currents. Deposits of FA 2.2 are interpreted as gravelly foresets with an important role of high-density turbidity currents and cohesionless debris flows. The facies subassociation FA 2.2 represents the coarsest part of the succession studied and is interpreted to be the proximal foresets i.e. close to the delta brink, and FA 2.1 as more distal foresets i.e. more basinward (Longhitano, 2008). The sandy foresets are probably derived from gravelly foresets (Eilertsen et al., 2011; Talling et al., 2012). Multiple alternations of foreset deposits with a strong dominance of low-density turbidites (i.e. FA 2.1) and foreset deposits with a significant role of debris flow deposits (i.e. FA 2.2) within the succession points to alternation of aggrading and prograding phases of the delta front (see Gobo et al., 2015) i.e. different A/S ratio (Kim and Chough, 2000) and also variations in the foreset angle (Kostic et al., 2002). The temporal changes indicated in the content of debris flow and/or high- and low-density turbidity current deposits could have been induced by climatic or tectonic allogenic factors influencing sediment dispersal to the delta front, which varied during delta evolution.

The prevalence of deposits of low-density turbidites generally suggest that sediment was mostly carried by hyperpycnal effluent bypassing the delta front (Turmel et al., 2015; Ventra et al., 2015; Dietrich et al., 2016).

FA 3 – TOESET DEPOSITS OF THE GILBERT-TYPE DELTAS

These deposits were recognized in only one exposure (Písečník) and consist of the tangential downdip terminations of foreset beds, interbedded with and overstepped by deposits of FA 2 (see Fig. 11B). Their base is not exposed.

Multiple scoop-shaped scours, 20 to 40 cm deep and a few metres wide, cross-cutting one another or pinching out both up-dip and down-dip, are filled by facies Sxu (see Fig. 11B). The base is concave and the top tabular to slightly convex. The scours are filled with cross-stratified to cross-laminated sand and fine pebble gravel with scattered small pebbles (up to 2 cm in diameter). Alternation of a few mm-thick laminae or a few cm-thick strata of fine, medium or coarse sandy layers and a few cm-thick layers of very coarse sand or fine pebble gravel is typical. Individual layers vary slightly in thickness. Adjacent scours frequently differ slightly in grain size of fill. Angular cross-stratification typically shows an upflow (relative to foresets) direction of inclination. The angle of the dip varies between 10 to 30° and might reveal upwards flattening.

The solitary beds of facies Sxu are interbedded with facies Gsa continuing from adjacent foreset (FA 2). Gsa within FA 3 differ in the bedding shape, bedding dip angle (typically 5–10°, i.e. significantly lower than in foreset beds) and partly/partially also in orientation of cross-stratification.

Interpretation: the scours are interpreted as produced by hydraulic jumps near the base of the slope (Massari and Parea, 1990; Nemec, 1990; Breda et al., 2007). Tangential decreases in steepness, genetic relation and position in the lower parts of the foresets suggest deposition in delta toeset settings. Sets of upflow/upslope (compared to adjacent foresets) dipping Sxu facies are interpreted as backsets. The spoon-shaped backset beds are interpreted as chute-and pool deposits or as deposits of cyclic steps (Okazaki et al., 2020). The Gsa beds covering the backset strata resulted from re-establishment of avalanching on foresets. A lower dip angle and some differences in the orientation of cross-stratification reflect the downflow flattening of strata. The overstepping of FA 3 by sub-parallel FA 2 beds reflects both progradation and aggradation of the depositional system.

FA 4 – BOTTOMSET DEPOSITS OF THE GILBERT-TYPE DELTAS

The transport of a large volume of sediment from the source area to the basin through a Gilbert-type delta depositional system commonly led to the development of a tripartite architecture (i.e. topset, foreset and bottomset; Gilbert, 1885). However, deposits which might be interpreted as bottomset are not described in either boreholes or exposures of the BS. A missing bottomset in the proximity of Gilbert-type delta nucleation and its evidence only in sections located farther basinwards are mentioned by Budai et al. (2021). Therefore, it is noticeable that several metre-thick heterolithic beds composed of centimetre- to decimetre-thick alternations of fine- to medium-grained sand and mud with isolated floating pebbles and cobbles (of granitoid, limestone, quartz, conglomerate, and mudstone intraclasts, i.e. with identical pebble composition as in the BS) were recognized in several boreholes (HJ 1 Chrlice, HJ 103 Opatovice) located in the southeasternmost part of the area under study (Hladilová et al., 2001), in the part of the WCF where typical BS were previously not recognized. Here, these beds are sandwiched between deposits of FA 6 (above) and by the Karpatian deposits of the Laa Fm. (below). The composition of pebbles from the Laa Fm. (borehole HJ 103) reveals significant differences to the composition the BS deposited above, with a very high content of carbonates, metamorphic and magmatic rocks and a lesser content of quartz, sandstones and cherts.

Interpretation: the position and sedimentary features of these beds suggest that they may represent the “missing” bottomset deposits of the BS deposited closer to the basinward delta pinchout. The stratified beds were deposited from low-density turbidity currents (Lowe, 1982) and the isolated larger clasts may result from coeval debris fall processes (Nemec et al., 1999) or individual clasts from transport in cohesionless debris flows (Sohn et al., 1997).

The lack of bottomset deposits (“trapezoidal delta” of Poulimenos et al., 1993) might be explained by sediment storage upstream from the bottomset area, especially as delta evolution was in its early stages (Mortimer et al., 2005), by sediment bypass and/or erosion in the bottomset area (Rubi et al., 2018), or by a basin with dissected topographic highs (Zelilidis and Kontopoulos, 1996).

FA 5 – SHOAL-WATER DELTA DEPOSITS

This facies association is mostly composed of thin- to medium-bedded strata of planar parallel-laminated sands of facies Sl (43.9%) (Fig. 12A, E), very thin- to medium-bedded structureless sands of facies Sm (25.4%) (Fig. 12B), and thin- to medium/thick-bedded sands of fine to very fine-grained sands of facies Sc (18.5%) (Fig. 12D, E), which are characterized by the presence of plant and coal fragments or coal laminae. Thin- to medium-thick intercalations of conglomerates of facies Gsa (Fig. 12C) and of graded sands of facies Sg are rare, forming 7.7 or

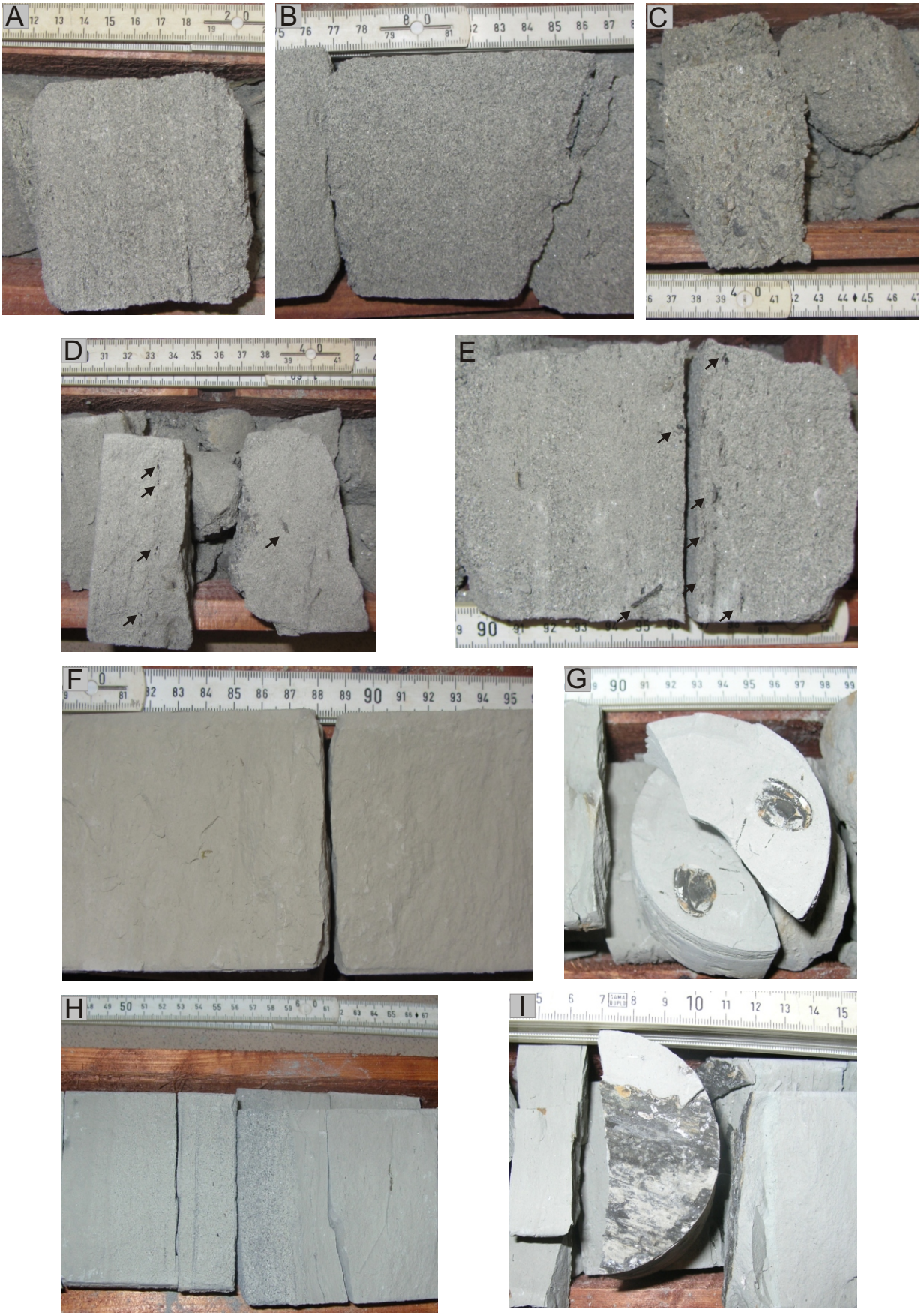

Fig. 12. Selected examples of lithofacies and facies associations of shoal-water delta and offshore marine deposits

A – lithofacies Sl (FA 5); **B** – lithofacies Sm (FA 5); **C** – lithofacies Gsa (FA 5); **D** – lithofacies Sc (FA 5) – intraclasts of coal or coal interlaminae are marked by black arrows; **E** – lithofacies Sl and Sc (FA 5) – intraclasts of coal or coal interlaminae are marked by black arrows; **F** – facies Mh (FA 6); **G** – facies Mm (FA 6); **H** – interbed of facies Sl within thick bed of lithofacies Mm (FA 6); **I** – enriched coalified plant fragment – laminae of lithofacies C within thick bed of lithofacies Mm (FA 6)

4.6% of FA 5. Contacts of the horizontal to subhorizontal beds are typically sharp and flat, commonly erosional. A significant grain size contrast between adjacent beds is typical. The deposits of FA 5 are arranged in fining- and then coarsening-upward strata sets and are significantly finer-grained and thinner-bedded than the underlying deposits of FA 2. They are overlain by mudstones of FA 6. FA 5 is identified only in the subsurface (22-41B borehole) where its thickness reaches ~7.1 m.

Interpretation: the dominant well-stratified sandstones of facies Sl, Sc and Gsa correspond to low-density turbidity currents, and in the case of facies Sc, with high suspended loads. These deposits alternate with high-density turbidites of facies Sm. Both high- and low-density turbidity currents are responsible for deposition of Sg. Common alternation of dominant lithofacies Sm and Sl, and the transition from massive to laminated division in facies Sg, reflect similar flow velocities but a decrease in the rate of sediment fallout, common in hyperpycnal flows (Zavala and Arcuri, 2006). The common occurrence of terrestrial plant remnants indicates a nearby terrestrial source. The high rate of fallout of sand-sized materials resulted in the trapping of transported plant debris. Bed geometry and bedset stacking points to retrogradation and then basinwards progradation of flat erosive bodies of density flows. From its spatial context, this facies association is thought to represent a shoal-water delta (Rasmussen, 2000) dominated by the emplacement of turbidity currents probably generated by river floods. The occurrence of coal and plant fragments suggests conditions suitable for peat formation in the nearby source area i.e. a poorly drained and generally flat floodplain with organic deposition in lagoons and/or marshes. Pulses of terrestrially derived organic debris entered the depositional system as a result of heightened river discharge.

FA 6 – OFFSHORE MARINE DEPOSITS

In the stratigraphic succession the mudstones of FA 6 sharply overlie the deposits of Gilbert-type delta foreset FA 2 (Fig. 5D), or rarely topset FA 1 deposits (Fig. 4A–C) or deposits of shoal-water delta FA 5, and are overlain by Quaternary deposits. The FA 6 facies association can be subdivided into two subassociations. The lower subassociation FA 6a is mostly (70.3%) composed of medium to thick beds of silty muds of facies Mh (Fig. 12F). Less common (16.2%) are thinly bedded massive, mollusc-bearing mudstones of facies Mm (Fig. 12G). Mudstones are rarely interspersed with thin to very thin (a few cm-thick) tabular beds of facies Sm, Sl or laminae of coalified plant fragments of facies C (Fig. 12H, I). Heterolithic bedding due to alternation of thin- to medium-thick beds with significant textural contrast is characteristic of FA 6a. FA 6a is only ~1.85 m thick and gradually transits into the monotonous FA 6b subassociation above. FA 6b comprises tens to hundreds of metre-thick (148 m thick in the borehole 22-41B) uniform mudstone successions of mostly massive Mm facies or significantly less commonly laminated mudstones of Mh facies. The mudstones are very thickly bedded, calcareous, rich in marine fossils and the index of bioturbation is generally low. Very thin to thin interbeds of facies Sl or Sb are extremely rare. The monotonous mudstones of FA 6b form the volumetrically predominant infill of the Lower Badenian succession of the WCF in general and are known as “Tegel” in the local lithostratigraphy.

Interpretation: the deposits of FA 6 represent an offshore sedimentary environment (Harms et al., 1982; Johnson and Baldwin, 1996) and a marine pelagic environment is indicated by its fossil content (Bubík et al., 2005, 2019).

The heterolithic bedding of FA 6a is interpreted resulting from deposition under variable flow conditions with mud deposition related to either increased suspended sediment concentrations or to mud flocculation. Cyclic fluctuations in both low to high energy conditions and sediment input are suggested by occurrences of parallel and lenticular silt laminae within the dominant Mh facies and also by episodic incursions of facies Sm, Sl and C. Facies Sm and Sl are interpreted as deposits of high- and low-density turbidity currents (Lowe, 1982) entering more distal parts of the basin. These were generated by river floods and/or by coastal slope-draining flash floods. The exclusively intrabasinal origin of coarse-grained particles (clay chips, shell fragments) in FA 6 differs markedly from the mix of extrabasinal and intrabasinal gravel clasts in FA 2 and FA 3. The bimodal grain-size distribution reflects simultaneous deposition of small and large particles and hyperpycnal flows capable of eroding the muddy substrate and transferring intrabasinal and extrabasinal organic matter into the distal parts of the basin. Locally abundant plant detritus suggests direct fluvial discharge into the basin and hyperpycnal flows. Rapid burial contributes to preserving the organic matter from oxidation (Zavala and Arcuri, 2006). Variable flow conditions, relations to hyperpycnal flows and paucity of tidal rhythmicity suggests possible seasonal cyclicity and precipitation that heightened river discharge, with hyperpycnal deposition in the distal parts of the basin (Zavala and Arcuri, 2006).

Mud content increase dramatically and rapidly upwards through FA 6 indicating an overall reduction of energy of depositional environment. The monotonous appearance of FA 6b could be evidence of a relatively more distal position to the terrigenous clastic input (compared to FA 6a) and suspension fallout deposition. However, transport of the mud into the basin might have been connected with river-derived hypopycnal suspension plumes (Nemec, 1995) and deposition via flocculation, signalled by the irregular laminae of dominant facies Mm in low-energy subaqueous settings (Weleschuck and Dashtgard, 2019). The very rare incursion of Sl and Sm facies are interpreted as deposits of both high- and low-density turbidity currents (Lowe, 1982) connected with hyperpycnal flows or with tempestites. Conditions were unfavourable for faunal colonization, as shown by the sparse trace fossils.

The sharp contact of basinal mudstones of FA 6 and Gilbert-type delta foresets of FA 2 (Fig. 5D), commonly without any preserved topset beds (FA 1) or shoal-water delta deposits (FA 5), indicate very rapid drowning of the delta, its retrogradation, a significant landward facies shift and a rapid increase in accommodation/sediment supply ratio.

AREAL DISTRIBUTION AND STRATIGRAPHIC ARCHITECTURE OF THE BRNO SANDS

The total thickness of the BS ranges from zero to >85 m (Fig. 13A) in the area under study, with the greatest thickness around borehole HV 102. The depositional record of the BS is predominantly formed by foreset beds. However, the identification of some other FA (especially FA 1, 3 or 5) is not possible from the archived borehole description.

The BS form an elongated sedimentary body markedly elongated NW–SE (~35 km) and narrower NE–SW direction (6–14 km), oriented almost perpendicular to the WCF Basin main axis. The shape of the BS sedimentary body resembles the infill of an incised valley. The thickness of the BS increases almost symmetrically from the margins into the centre of

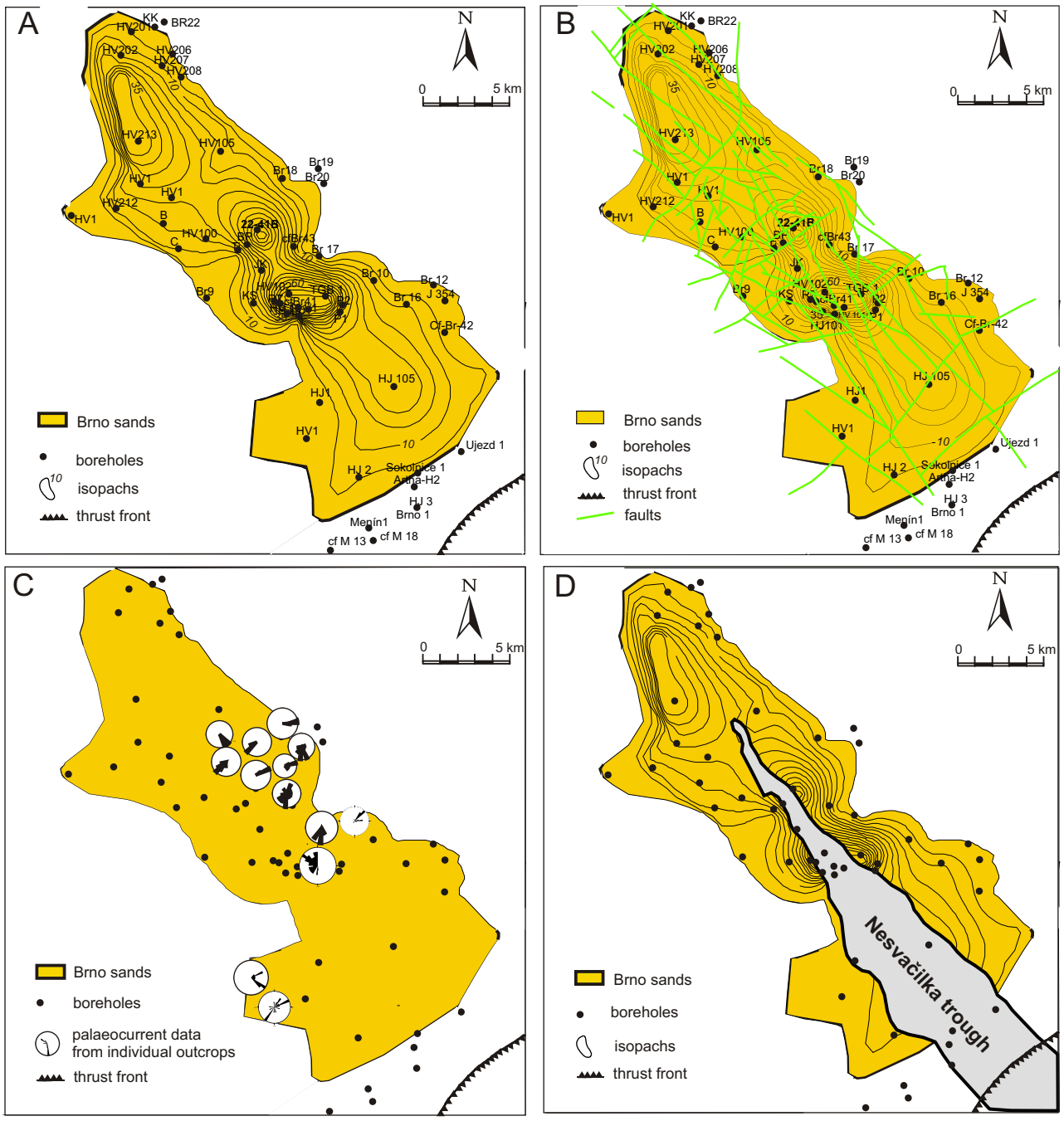

Fig. 13A – areal extent and map of thickness of the Brno sands; B – distribution of faults documented in study area (according to Hanžl et al., 1999; Krejčí et al., 2018) and map of thickness of the Brno sands; C – comparison of thickness and areal distribution of the Brno sands and palaeocurrent data; D – spatial relation of thickness and areal distribution of the Brno sands and areal extent of the Paleogene Nesvačilka palaeovalley

palaeovalley, where ~3 depocentres can be recognized oriented parallel to its NW–SE axis. Rapid increase of BS thickness can be followed from both NE and SW margins especially into the depocentres. A significant trend of BS thinning towards the WCF Basin i.e. towards the SE, where the bottomset deposits of FA 4 are interpreted, is also notable.

Such a situation points to a significant role of tectonics in the formation of the accommodation space for the BS. Both the orientation of the BS-filled palaeovalley and the position of individual depocentres coincides well with the distribution of faults documented by geological mapping (Hanžl et al., 1999; Krejčí et al., 2018) as shown on Figure 13B.

The areal distribution and thickness of the BS can be compared with palaeocurrent directions which are determined mostly from the foreset dips (see Fig. 13C). Although the interpretation of palaeocurrent data might be partly affected by the distribution of the available exposures, they provide overall uniform results. Localities along the NE margin of the valley point to dominant transport towards the palaeovalley i.e. to the W, SW, S or SE. Similarly, localities along the SW margins show transport direction towards the NE or E i.e. into the central parts of the palaeovalley. Transport direction along the palaeovalley axis plays a minor role.

Interpretation: the geometry of the palaeovalley and its infill are strongly controlled by tectonics. The accommodation space for the BS is tectonically influenced by mostly NE–SW trending basement faults. The palaeovalley is located in the most proximal parts (NW) of the NW–SE oriented Nesvačilka trough/palaeovalley known from the subsurface of the WCF and filled with Paleogene deposits (Fig. 13D). The Nesvačilka palaeovalley is interpreted as a morphological depression of erosional origin, with tectonic control (Pícha, 1979; Jiříček, 1987; Pícha et al., 2006). The specific structural setting of the BS-filled palaeovalley, with margins commonly bordered by faults, affects the morphology and the depositional settings of the BS. Gilbert-type deltas are generated mainly along NW–SE trending major faults, while NE–SW trending minor faults contributed to the lateral development of the depocentres and to the basin-fill configuration.

The thickness of Gilbert-type deltas is a direct measure of the sum of:

- initial depth of the water body into which the delta was built;
- changes in basin depth through deposition, which may be due to relative base-level rise or delta progradation into deeper basin areas.

The architectural expression of this is manifested in basinwards delta-foreset growth (Budai et al., 2021).

Gilbert-type delta slopes archive an increase in thickness through delta progradation of several kilometres basinward. Transport of sediment was often perpendicular to the palaeovalley axis, i.e. mostly from the NE margin towards the SW, S and SE and also from the SW margin towards the N and NE. An axial direction of progradation, i.e. from NW towards SE, was also partly recognized but seems to be less pronounced. Although palaeocurrent directions could vary substantially from one deltaic sequence to the next, the direction of input into depocentres eventually prevailed. The distribution of clinoforms along palaeovalley margins resembles the delta-fed aprons of Galloway (1998) i.e. laterally extensive deposits fed by line source systems. One system of Gilbert-type deltas was developed along the NE margin of the palaeovalley and a second one along its SW margin. The role of these systems probably changed in time as did the position of the individual deltaic bodies' nucleation.

Abrupt changes in basement geometry resulting in significant changes in the foreset thickness are typical:

- close to the point of the landward delta nucleation i.e. along the palaeovalley NE and SW margins;
- during progradation over faulted basement or inherited depositional or erosional topography i.e. into depocentres.

Rapid increase in the BS thickness (doubling or tripling over a horizontal distance of several hundred metres) can be followed especially in connection with the SE-most depocentre. The morphology and relative variations in formation of accommodation space are supposed to predispose the existence of depocentres oriented almost linearly along the valley axis. Inherited topography could have played a role by creating differential accommodation space. The contrasts between the trajectories along different parts/localities of the palaeovalley could have resulted from local sediment supply variability or from inherited basin physiography.

PROVENANCE ANALYSIS

Gilbert-type deltas form important bundles in sediment-delivery pathways linking continental hinterlands to basin depocentres. Catchment-area bedrock and physiography represents one of the allogenic factors that influence delta evolution. Provenance analysis is based on pebble petrography, analyses of heavy minerals, and garnet and rutile composition.

PETROGRAPHY OF PEBBLES AND COBBLES, SHAPE AND ROUNDNESS OF PEBBLES

The gravels can be classified as polymict. Significant differences in the content of individual lithologies in the pebble spectra were initially recognized by Krystek (1974). Quartz pebbles represent a stable component, forming 4.0–41.0% of the pebble spectra. Metamorphic rocks are mostly represented by gneisses, quartzites, mica-schists, metabasites or phyllites forming 10 to 49%. Pebbles of magmatic rocks (granitoids, aplites) form 0–32%. The content of pebbles of sedimentary rock types varies between 14 and 56%. The proportion of individual sedimentary rocks (i.e. sandstones, arkoses, limestones/both Paleozoic and Jurassic ones, greywackes, shales, cherts, spongolites) in individual localities varies similarly. The occurrence of limestones is especially unstable. The proportion of mudstone (silty clays) intraclasts can exceed 10% of the pebble spectra. The intraclasts are typically significantly larger than the associated extraclasts, some approaching 1.2 m in size (see Fig. 9A).

Vertical variations in the pebble spectra were studied within the 64 m thick succession of the 22-41B borehole. Quartz pebbles represent a stable component forming 5.3–51.5% of the pebble spectra. Various varieties of quartz are present (whitish, milky, light or dark grey, pinkish and yellow). Quartz clasts are mostly spheres (25–57.7%) and/or blades (25–60.6%). The content of discs (1.5–12.2%) and rods (0–12.1%) is significantly lower. Clasts are mostly subangular (29.3–68.2%) and subrounded (14.8–48.2%). The content of angular or rounded quartzes is lower. Clasts of magmatic rocks (mostly granitoids, rarely aplites) form 19.4–52.6%. Pebbles of granitoids are mostly spherical (30.2–70.8%) and/or bladed (15–66.6%) in shape, typically angular (30–73.3%) or subangular (23.1–70%). Rounded pebbles of granitoids were missing. The proportion of metamorphic rocks (mica-schists, metabasites, gneisses, quartzites, phyllites, schists) varies widely (0.6 to 39.5%) in the pebble spectra. Pebbles of mica-schists are mostly discs or blades and they are typically subangular to subrounded. Sedimentary rocks (sandstones, limestones, shales, cherts) represent 0 to 33.9% of the pebble spectra.

Some differences in the content of individual rocks by comparison with data from exposures are influenced by varied grain size (with borehole samples being generally smaller than ones from exposure). The mudstone intraclasts are often especially difficult to quantify in borehole cores of loose gravelly sand.

HEAVY MINERALS

Heavy minerals are sensitive indicators of provenance, weathering, transport, deposition and diagenesis (Morton and Hallsworth, 1994) especially if combined with the chemistry of selected heavy minerals (Morton, 1984). The ZTR (zircon + tourmaline + rutile) index is widely accepted as a criterion for the mineralogical "maturity" of heavy mineral assemblages (Hubert, 1962; Morton and Hallsworth, 1994) in the case of derivation from a similar source.

The BS possess relatively stable heavy mineral assemblages where garnet always dominates in the heavy mineral spectra, its content varying between 62.5 and 88%. Epidote,

amphibole, staurolite and apatite are subsidiary heavy minerals. All other heavy minerals recognized (disthene, rutile, zircon, tourmaline, titanite, anatase, glaucophane, monazite, andalusite, and sillimanite) are accessory. The value of the ZTR index is low, ranging between 1.9 and 7.

Garnet and rutile represent common heavy minerals in the deposits studied, being relatively stable in diagenesis and having a wide compositional range, thus enabling further evaluation in detail.

COMPOSITION OF GARNET

The chemistry of detrital garnet is widely used for the more detailed determination of source rocks (Morton, 1984). A relatively broad spectrum of eleven garnet types was recognized for the BS (see Table 2). However, only four types are more common and a strong dominance of almandines is evident. Almandine generally reveals a primary source from metamorphic rocks such as gneisses or granulites. Although grossular or spessartine garnets form only a few percent of the garnet spectra, they give information about the occurrence of skarns, crystalline limestones, pegmatites or granitic rocks in the source area.

Multivariate analysis of garnet chemistry according to Tolosana-Delgado et al. (2018) recognize four sources of garnet (see Fig. 14A, B). The predominant source was from amphibolite facies metamorphic rocks (66.4–74.6%). Sources derived from granulite facies metamorphics (16.7–31.2%) or eclogite facies metamorphics (21.5%) were less important. Garnets from igneous rocks (2.4%) were only accessory and an ultramafic source was not recognized.

Several ternary discrimination diagrams are utilized for more detailed identification of the primary source of garnet (Fig. 14C–E). The PRP–ALM+SPS–GRS diagram (Mange and Morton, 2007) in Figure 14C reflects the dominant source of garnets from amphibolite facies metasedimentary rocks (67.4%) and intermediate to felsic igneous rocks (25.9%). Significantly less common are garnets from high-grade mafic rocks (4.4%) or high-grade granulite facies metasedimentary rocks (2.2%).

The PRP–ALM–GRS diagram (Aubrecht et al., 2009) in Figure 14D indicates the overwhelmingly dominant primary source of garnets to be from amphibolite facies rocks (especially gneisses and amphibolites). Significantly less common are garnets from felsic and intermediate granulites. Other possible sources (igneous rocks, skarns, serpentinites) are also less common.

Diagram GRS–SPS–PRP (Fig. 14E) enables a comparison with the potential source rocks of the eastern margin of the Bohemian Massif (cf. Otava et al., 2000; Čopjaková et al., 2002). Althought the results are complex, the predominant part of the garnets could have originated from the Moravian Unit. The Moldanubian Unit and granitoids of the Brno Massif could also represent a source of a minor part of the garnets studied, similarly to the Moravian-Silesian Paleozoic/Culmian rocks and the Svratka Crystalline Complex.

Table 2

Garnet types recognized in the Brno sands

Garnet type	[%]
$ALM_{53–84}PRP_{11–45}GRS_{0–9}SPS_{1–7}AND_{0–3}$	13.3
$ALM_{57–85}GRS_{11–31}PRP_{2–9}SPS_{1–9}AND_{0–2}$	36.7
$ALM_{76–85}GRS_{2–9}PRP_{4–9}SPS_{0–9}AND_{0–2}$	11.1
$ALM_{55–74}GRS_{13–24}PRP_{11–18}SPS_{0–8}AND_{0–2}$	15.6
$ALM_{42–67}SPS_{12–40}PRP_{11–16}GRS_{1–9}AND_{0–2}$	1.1
$ALM_{47–71}GRS_{13–27}SPS_{11–19}PRP_{4–8}AND_{0–4}$	3.3
$ALM_{57–76}SPS_{11–26}Prp_{0–10}AND_2GRS_{3–9}$	5.5
$ALM_{57–75}PRP_{12–28}GRS_{11–22}SPS_{0–9}AND_{0–2}$	8.8
$ALM_{51–75}SPS_{21–23}GRS_{10–19}PRP_{2–9}AND_{0–2}$	2.2
$GRS_{57}AND_{27}PRP_{15}$	1.3
$SPS_{45–64}ALM_{22–41}PRP_{0–6}AND_{0–4}GRS_{3–9}$	1.1

COMPOSITION OF RUTILE

Rutile as an ultrastable mineral is commonly used for provenance studies (Force, 1980; Zack et al., 2004a, b; Triebold et al., 2007).

The concentrations of the main diagnostic elements (Fe, Nb, Cr and Zr) vary significantly for the samples studied. The content of Fe shows that all analysed rutiles come from metamorphic rocks. The concentration of Nb ranges between 172 and 13800 (average 3348 ppm), the concentration of Cr varies between 55 and 3540 ppm (average 513 ppm), the concentration of Zr ranges between 28 and 237 ppm (average 57 ppm) and most (86.2%) of the logCr/Nb values are negative. A great majority (89.7%) of metamorphic rutiles from the BS originate from metapelites (mica-schists, paragneisses, felsitic granulites) and only a few (10.3%) originate from metamafic rocks (eclogites, basic granulites), according to the grouping by Zack et al. (2004a, b) or Triebold et al. (2007). According to the diagnostic criteria of Triebold et al. (2012), 86.2% of the rutiles originate from metapelites and 13.8% from metamafics. A discrimination plot of Cr *versus* Nb is shown in Figure 15.

The results of Zr-in-rutile thermometry (applied to metapelitic rutiles only – see Zack et al., 2004 a, b; Watson et al., 2006; Meinhold et al., 2008) indicate that rutiles from the BS originate mostly from medium-temperature metamorphic rocks (amphibolite metamorfic facies), less commonly from low-temperature metamorphics (green schists).

INTERPRETATION OF THE PROVENANCE DATA

A combination of techniques used in evaluation of the source area enables the evaluation of both a “primary” source from crystalline units and a “secondary“ source redeposited (often multiple) from sedimentary units.

Polymict gravels with some variations (both areal and vertical) in the pebble spectra together with variations in pebble shape and roundness point to the varied role of local factors/sources and multiple redeposition of the material both from primary and secondary sources. The results of heavy mineral analyses together with the compositions of garnet and rutile demonstrate the importance of metamorphic rocks in the source area. Provenance can be located in the nearby Brno Massif and its sedimentary cover i.e. especially siliciclastic rocks (“Culmian facies”) of the Moravian-Silesian Paleozoic, but also from the Devonian siliciclastics (Old Red facies) and in Cretaceous deposits. Similarly, a source from crystalline units of i.e. Moravian, Moldanubian Units and Svratka Complex which are located slightly more to the W was indicated.

Material redeposited from the Lower (Ottnangian, Karpatian) and Middle Miocene (Lower Badenian) infill of the WCF

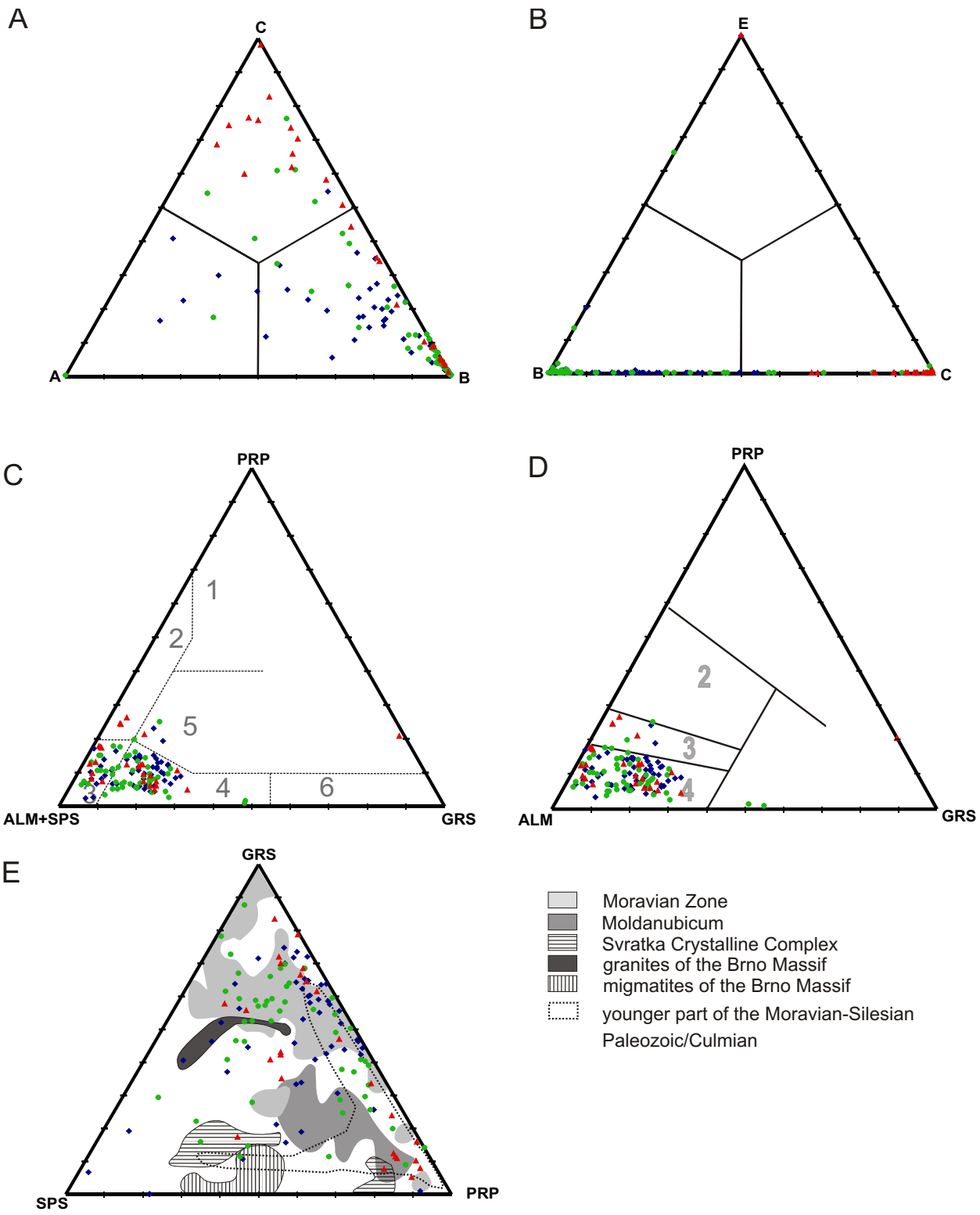

Fig. 14. Ternary diagrams of the chemistry of detrital garnets

A – ternary diagram based on multivariate analysis according to Tolsana-Delgado et al. (2018) (A – eclogite facies, B – amphibolite facies, C – granulite facies); **B** – ternary diagram based on multivariate analysis according to Tolsana-Delgado et al. (2018) (B – amphibolite facies, C – granulite facies, E – igneous rocks); **C** – discrimination diagram according to Mange and Morton (2007) (1 – pyroxenites and peridotites, 2 – high-grade granulite facies metasedimentary rocks and intermediate felsic igneous rocks, 3 – intermediate to felsic igneous rocks, 4 – amphibolite facies metasedimentary rocks); **D** – discrimination diagram according to Aubrecht et al. (2009) (1 – pyroxenites and peridotites, 2 – felsic and intermediate granulites, 3 – gneisses and amphibolites metamorphosed under pressure and temperature conditions transitional to granulite and amphibolite facies metamorphism, 4 – gneisses metamorphosed under amphibolite facies conditions; 5 – mainly from high-grade mafic rocks, 6 – metasomatic rocks); **E** – ternary diagram of the chemistry of detrital garnets in comparison with possible source areas; ALM – almandine, GRS – grossular, PRP – pyrope, SPS – spessartine; data from source rocks according to Otava et al. (2000), Čopjaková et al. (2002, 2005), Čopjaková (2007) and Buriánek et al. (2012)

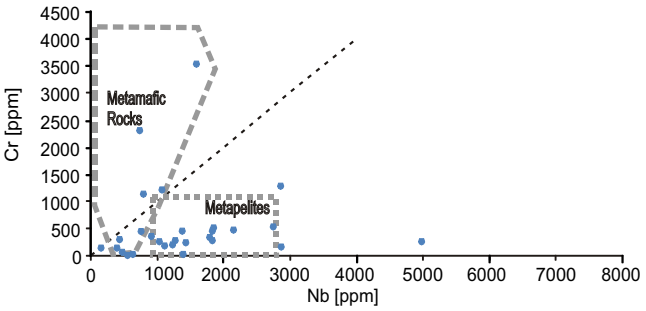

Fig. 15. Discrimination plot of Cr *versus* Nb of the rutiles investigated

also played an important role. This source is recorded both as mudstone intraclasts, and also by palaeontological data (Bubík and Petrová, 2004; Buriánek et al., 2012). Abundant intraclasts suggest enhanced erosion of subaerially exposed distal offshore deposits associated with significant relative sea level fall. Redeposition from the Lower Badenian basinal mudstones ("Tegel") points to an "older" Lower Badenian cycle of relative sea level change in the area under study. The deposits of this cycle have mostly been eroded. Generally, a low ZTR index does not deny the role of redeposition but more probably reflects a little reworking of material before erosion by the BS depositional system.

The provenance data obtained can be summarized as indicating that the source area of the BS clearly points to the nearby geological units. Some variations in provenance are explained by local/regional differences in bedrock geology. There was no systematic trend within the source area of the depositional system of the BS.

DISCUSSION

The Brno sands are interpreted absolutely predominantly as deposits of Gilbert-type deltas. Although classical depositional elements (topset, foreset, toeset and bottomset) were recognized within the Gilbert-type deltas studied, they can be classified as foreset-dominated because their architecture is governed by a thick delta foreset with much less representation of other elements (Edmonds et al., 2011; Viparelli et al., 2012). The deltas forced forward-stepping (basinwards) into a confined palaeovalley (i.e. towards the SW, S, SE, E, N and NE). A combination of longitudinal and transverse inputs is inferred; however, their role probably varied in time and space. The clinoforms are laterally extensive in plan view, forming progradational wedges. The important role of basin margin morphology with localized sediment supply through several drainage systems is reflected by the complex provenance of the BS from geological units near the palaeovalley and its older sedimentary infill, and in the spatial variations in the pebble composition (see Krystek, 1974). However, variables of individual feeders were diminished within the incised valley depositional system. Schematic reconstruction of the palaeogeographical situation associated with the filling of the studied palaeovalley by the Brno sands and a correlation panel showing the spatial relationship

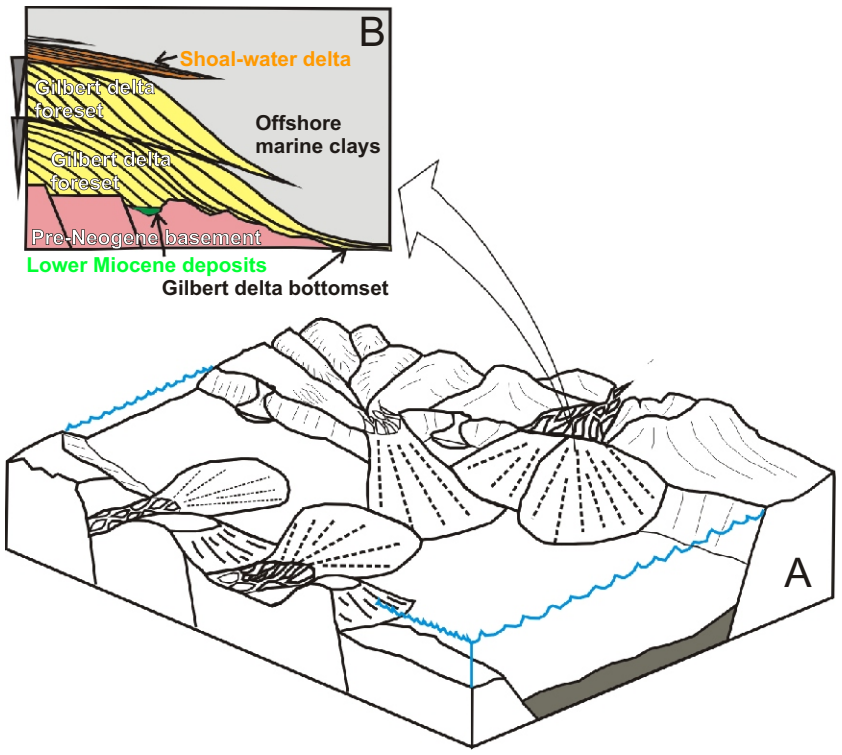

Fig. 16A – schematic reconstruction of the palaeogeographical situation showing filling of the palaeovalley studied by Gilbert-type delta system of the Brno sands; B – schematic correlation panel showing the spatial relationship between the Brno sands and the non-deltaic Neogene succession within the palaeovalley

between the Brno sands and non-deltaic Neogene succession within the palaeovalley are shown in Figure 16.

The stratigraphic arrangement of the generally fining-up and deepening-up Middle Miocene sedimentary succession within the confined palaeovalley provides a record of the interplay between available accommodation space (A), and sediment supply (S), expressed as the "A/S ratio" (Postma, 1984; Jervey, 1988; Muto and Steel, 1997; López-Blanco et al., 2000; Breda et al., 2009; Backert et al., 2010; Gobo et al., 2014). Four recognizable stages of valley evolution, connected with significant changes in the A/S ratio, can be identified, together with a few subsidiary episodes.

Stage A: the location of the palaeovalley on the forebulge basinward flank suggests that the valley accommodation space was controlled by both tectonics and eustatic sea level changes (Gawthorpe and Collela, 1990; Catuneanu et al., 1998; Catuneanu and Sweet, 1999; Blum and Tornqvist, 2000; Bruhn and Steel, 2003; Leszczyński and Nemec, 2015) with the additional roles of palaeotopography, geology of the drainage basin and climate (Shanley and McCabe, 1994; Gupta, 1999; Viseras et al., 2003; Andreucci et al., 2014). The role of the principal individual factors recorded in the sedimentary history of the palaeovalley varied.

The formation and evolution of the WCF are generated by increased crustal loading associated with a thickened orogenic wedge propagating generally towards the NW. As thrust loading increased, the mechanical strength of the basement was exceeded and fault activity enhanced along zones of basement weakness (Waschbusch and Royden, 1992). The rheologic anisotropy along the eastern margin of the Bohemian Massif formed by several NW–SE trending faults significantly influences the WCF basin extent and facies distribution (Nehyba et al., 2019; Blaško and Nehyba, 2020). Here, the confined palaeovalley developed within the forebulge zone along NW–SE trending basement faults, hosted in crystalline bedrock and its sedimentary cover, almost perpendicular to the WCF basin main axis. However, the accommodational activity of these faults is already documented in the area under study by Paleogene deposits of the Nesvačilka palaeovalley, or more precisely its NW termination. Older Neogene deposits of the WCF recognized in the palaeovalley (Ottnangian, Karpatian in age), which underly the BS, show that the area was flooded before the deposition of BS. However, their relic preservation points to an erosion phase/phases and signal re-entrenchment of the valley. The incision of the palaeovalley prior to the deposition of BS was connected with Early/Middle Miocene sea level fall (e.g., Hoheneger et al., 2014). The onset of valley incision tends to commence when a convex-up topography is exposed during relative sea level fall (Wang et al., 2019). The re-entrenchment of the confined palaeovalley was accompanied by the formation of a steep base level profile and base level fall (negative accommodation). A high rate and magnitude of relative sea level fall is inferred in forming the incised valley, with intense erosion.

The erosional base of BS is considered as a sequence boundary/basal unconformity of the Middle Miocene valley succession. This polygenetic surface originated from both subaerial and marine erosion. The palaeovalley was bordered by tectonically active and steep margins. Basement structural anisotropy associated with several systems of NW–SE and NE–SW faults led to formation of parallel aligned basement blocks with different subsidence rates. The role of these faults for the WCF basin shape and morphology has been documented (Cogan et al., 1993; Eliáš and Pálenský, 1998; Francírek and Nehyba, 2016; Nehyba et al., 2019). Complex basement morphology affected the transportation and drainage pattern, and the position, type and size of both feeders and depocentres of BS (especially adjacent to the junction of fault systems).

Stage B: this stage reflects the switch from incision and erosion to sediment accumulation. The first marine invasion drowned the palaeovalley floor relief produced by the preceding phases of valley evacuation. The absence of transgressive deposits might indicate very rapid relative sea level rise ("non-accretionary" transgression *sensu* Helland-Hansen and Gjelberg, 1994).

Marginal slopes descended towards the central deeper parts of the palaeovalley over a distance of several kilometres. These slopes were incised by gullies and canyons, some of which were occupied by deltas and possibly also by alluvial fans. A high rate of sediment supply and steep palaeovalley margins under tectonic control resulted in formation of system of large-scale Gilbert-type deltas and their progradation.

The sediment supply was high and rapid enough to keep a steep front and slope of the delta, to form a thick sedimentary succession and to eliminate signals of reworking by waves or tides. This implies that relative sea level rise was superimposed on the synsedimentary activity of palaeovalley border faults (Massari and Colella, 1988). This would have produced a distinctive stratigraphic arrangement of depositional systems with thicker deposits in the internal parts of the palaeovalley and thinner ones along its margins. Tectonic subsidence creates accommodation space at high rates during the early stage of subsidence, and then accommodation space slowly increases with decreasing rate of subsidence. Tectonic subsidence also increases sediment supply by rejuvenating the drainage basin, but with a lag time. These changes in accommodation space and sediment supply in response to tectonic subsidence generally result in the deposition of fine-grained sediment during the early stage with a subsequent coarsening-upward trend with decreasing A/S ratio.

A/S changes are connected both with fault activity (responsible for "continuous" high sediment supply) and with relative sea level rise (responsible for a "continuous" rise of accommodation space) enabling a deltaic system to keep pace with rising relative sea level. The high sediment supply is further signalled by the prevalence of turbidite-dominated deposits within FA 2, which signal that the delta-front accommodation is at a minimum and sediment tends to be flushed downslope by erosional hyperpycnal flows (Gobo et al., 2015).

Although Gilbert-type deltas generally represent highly constructive, dominantly progradational systems (Nemec, 1990; Longhitano, 2008), their settings in detail primarily depend on the A/S ratio (Helland-Hansen and Martinsen, 1996; Steel and Olsen, 2002). The thick foreset deposits of BS reveal, in detail, repetitive variations in this ratio (e.g., successive prograding-retrograding episodes). These are interpreted as rapid high-frequency pulses of relative sea level change, expressed as vertically stacked deltaic wedges, and can be used for the evaluation of facies architecture and stacking pattern of the Gilbert-type deltas studied.

Deposits of the first episode of deltaic succession directly overlie the pre-Middle Miocene basement and are characterized by FA 2.1 overlain by FA 2.2. An increase in debris-flows in proximal parts of the delta slopes and turbiditic deposits in the distal parts has been recognized for Gilbert-type deltas in general, as was a coarsening-upward succession (Budai et al., 2001). Therefore, the arrangement of distal foreset deposits (FA 2.1) overlain by proximal foreset ones (FA 2.2) signal a forward-stepping progradational and aggradational stacking pattern, which is generally consistent with sediment overload-

ing/low rates of A/S ratio. These deposits are interpreted as representing a highstand systems tract (HST).

The superimposed part of the deltaic deposits is again characterized by a repeated FA 2.1–FA 2.2 succession and lies directly on the deposits of the first episode (i.e. on lower FA 2.2). The superposition of the distal parts of deltaic foresets over proximal ones indicates a retrogradational stacking pattern and is interpreted as evidence of TST. Retrogradation is consistent with sediment relative undersupply, i.e. higher rates of the A/S ratio. Although transgressive deposits were not recognized within the depositional succession, they might be signalled by the occurrence of mudstone intraclasts within the foreset beds.

The onset of Lower Badenian/Langhian deposition on the distal/cratonward margin of the WCF is typically recorded in two areally/laterally restricted successions overlying the Pre-Badenian basement:

- basal coarse clastic deposits (such as the BS) overlain by offshore marine muds;
- basement directly covered by offshore marine muds.

Because the coarse clastic deposits are partly coeval with the offshore muds (Bubík et al., 2019), this situation along the coastline is attributed to variations in coastal morphology and sediment supply. The deltaic shoreline, as within the palaeovalley, was characterized by high and localized sediment supply, which resulted in a more pronounced relative sea level rise and delayed flooding. In non-deltaic shoreline settings, the principal role is connected with the relief. The low-gradient relief was rapidly drowned with pronounced flooding of the backshore, whereas a high coastal relief could have prevented significant landwards shift of the shoreline and enable the recognition of transgressive conditions in the facies record (Ghinassi, 2007), promoting accretionary and non-accretionary transgressions (Helland-Hansen and Gjelberg, 1994). Therefore, diachroneity in the onset of Early Badenian/Langhian marine transgression is developed in deltaic and non-deltaic parts of the palaeovalley.

The sedimentary succession of the second episode itself (i.e. FA 2.1–FA 2.2) is interpreted as a progradational and aggradational stacking pattern, reflecting sediment overloading/low rates of the A/S ratio and consideration as (HST) deposits. The identical depositional architecture of the two superimposed deltaic episodes is interpreted as repetition of high-frequency cycles of relative sea level changes i.e. as high-frequency depositional sequences. Deposits of the lower sequence are significantly thicker (38.7 m) than deposits of the upper sequence (17.0 m).

However, spatial/ temporal variations in the stratal stacking patterns can be also driven by such factors as delta-lobe switching or climatically driven variations in sediment input (Colella, 1988; Elliott, 1989; Breda et al., 2007; Longhitano, 2008). The dimensions of the deltaic deposits studied, similarities in facies content, grain-size and gamma ray spectra (Dostalíková et al., 2018) exclude climate variations as the responsible agent. Lobe switching might be signalled by significant variations in palaeocurrent directions of deltaic sequences due to the lateral shift of lobes to different depocentres through time (Postma, 2001). Missing palaeocurrent data from the borehole did not allow the testing of this factor. The hypothesis of high-frequency sea level changes that influenced the BS stacking pattern is thus preferred.

The high sediment discharge and topographically restricted confinement minimize sediment dispersal and boost sediment aggradation and progradation through the palaeovalley and determine a Gilbert-type delta architectural element development and distribution. Different delta frameworks with various proportions of individual architectural elements might have been developed within various parts of the palaeovalley and the occurrence of topsets and bottomsets can be partly used for palaeogeographical purposes. The preservation of the topset is connected with the final episode of Gilbert-type delta deposition and simultaneously with its most landward occurrence. Evidence of bottomsets points to the most basinward reach of deltas.

Stage C: the transition from Gilbert-type to shoal-water type represents the final stage of deltaic deposition. The gradual sea level rise, high sediment supply and aggradation of proximal Gilbert-type delta deposits (i.e. the upper FA 2.2 package) within the confined palaeovalley led to the flattening of the feeder profile and partial reduction of sediment delivery. The indicated decrease in accommodation coupled with lower rates of sediment supply is interpreted as a response to a decline in tectonic activity along the palaeovalley margins (García-García et al., 2006; Eilertsen et al., 2011), reflected by deposition of a shoal-water delta. Reduction in the grain size and thickness of FA 5 (compared to FA 2) points to retrogradation of the feeders progressively upstream contemporaneously with continuing marine flooding of the forebulge and a cratonwards shift of the facies belts towards the source areas. An increase in the A/S ratio is inferred when compared with stage B. However, the shoal-water delta was recognized only in one borehole. Therefore, local factors might be important for its development or preservation.

Stage D: the BS deposits were overlain and overstepped by the transgressive succession represented by a thick pile of offshore marine muds, which indicate further inundation of the palaeovalley. Stage D represents a continuation (see stage C) of marine transgression (base-level rise) onto the WCF distal margin. In a coastal setting of low topographic gradient, such as the delta plain of a shoal-water delta, the relative rise in sea level will result in a major landwards shift of the shoreline (coastal onlap onto the foreland plate), accompanied by a marked decline in sediment supply (Ghinassi, 2007). The common sharp upper contact of BS and overlying offshore clays (marked by a significant decrease in sediment grain size) clearly reveal a rapid reduction of coarser-grained sediment supply, rapid increase of accommodation space, rapid flooding and ultimate drowning of the deltaic system. Marine invasion with a shift of the coastline further landwards led to a significant enlargement of the basin (far beyond the palaeovalley).

The Early Badenian evolution of the WCF is in general characterized by NW-directed, stepwise transgressions onto the basin margin, followed by stationary or even regressive phases (Nehyba et al., 2016; Holcová et al., 2018). The data presented support an overall trend of transgression of neritic facies onto the distal foreland margin, which occurred as rapid steps (probably of tens of kilometres).

Several episodes of flooding recognized within the succession point to a complicated depositional history of the WCF during the Early/Middle Miocene transition where eustatic sea level fluctuations superimposed on the dominant flexural background subsidence were locally accelerated by normal faulting (Haq et al., 1988; Miller et al., 1998; Allen et al., 2001).

CONCLUSIONS

The Middle Miocene (Lower Badenian) Brno sands in the southern part of the Western Carpathian Foredeep are interpreted predominantly as Gilbert-type delta deposits filling an incised valley defined by NW–SE trending faults, hosted in the

crystalline basement that formed the southern margin of the Bohemian Massif. Repeated accommodational activity of these faults/re-entrenchment of the palaeovalley is documented in the area studied since the Paleogene. The location of the palaeovalley on the forebulge basinward flank (almost perpendicular to the basin main axis) suggests that the accommodation space was controlled by both tectonics and eustatic sea level changes with the additional role of palaeotopography and climate.

The Gilbert-type deltas recognized can be classified as foreset-dominated, because their architecture is governed by thick delta foresets with much lesser representation of other elements (i.e. topsets, toesets and bottomsets). The deltas forced forward-stepping (basinwards) into a confined palaeovalley (ie. towards the SW, S, SE, E, N and NE). One system of deltas developed along the NE margin of the palaeovalley and the second one along its SW margin. The foreset beds reflect a prevalence of low-density turbidites, with varied but important evidence of high-density turbidites, deposits of cohesionless debris flows and debris falls. The thickness of the Brno sands increases almost symmetrically from the margins into the centre of palaeovalley, which indicates progradation of deltas several kilometres basinwards.

The erosional base of the Brno sands is considered as a sequence boundary/basal unconformity of the Middle Miocene valley succession. This polygenetic surface originated from both subaerial and marine erosion. The nucleation of Gilbert-type deltas was connected with a lowstand. The thick foreset deposits reveal, in detail, repetitive successive prograding-retrograding episodes. These are interpreted as rapid high-frequency pulses of relative sea level change i.e. as high-frequency depositional sequences.

The deltaic deposition of the Brno sands was terminated by deposits of a shoal-water delta and the sands were finally drowned by offshore pelagic muds. The stratigraphic arrangement of the generally fining-up and deepening-up Middle Miocene sedimentary succession within the confined palaeovalley reveals a rapid reduction in the coarser-grained sediment supply, a rapid increase of accommodation space, rapid flooding and ultimately the flooding of the basin foreland margin.

Provenance analysis based on the pebble petrography, analyses of heavy minerals, garnet and rutile composition recognise some variations in the polymict Brno sands both areally and within their succession. These variations are explained by the varied role of local sources, variations in local bedrock geology, and multiple redeposition. The provenance of the Brno sands is located in nearby geological units such as the Brno Massif and its sedimentary cover (especially Paleozoic and Cretaceous deposits), together with sources from crystalline geological units of the Moravian, Svratka Crystalline and Moldanubian Units, which are located slightly more to the W. An important role was played by material redeposited form the Lower (Ottnangian, Karpatian) and Middle (Lower Badenian) Miocene infill of the Western Carpathian Foredeep.

Acknowledgements. The study was kindly supported by the institutional support of Masaryk University Brno (project 1363). The author would like to thank the Czech Geological Survey – Brno branch for permission to study cores of the borehole 22-41B Brno – Černá Pole. Two anonymous reviewers are thanked for valuable advice and useful comments on the manuscript.

REFERENCES

Adámek, J., 2003. Miocén karpatské předhlubně na jižní Moravě, Geologický vývoj a litostratigrafické členění (in Czech). Zprávy o geologických výzkumech v roce 2002: 9–11.

Allen, P.A., Burgess, P.M., Galewsky, J., Sinclair, H.D., 2001. Flexural-eustatic numerical model for drowning of the Eocene perialpine carbonate ramp and implications for Alpine geodynamics. GSA Bulletin, **113**: 1052–1066.

Andreucci, S., Panzeri, L., Martini, P., Maspero, F., Martini, M., Pascucci, V., 2014. Evolution and architecture of a West Mediterranean Upper Pleistocene to Holocene coastal Apron-fan system. Sedimentology, **61**: 333–361.

Aubrecht, R., Méres, Š., Sýkora, M., Mikus T., 2009. Provenance of the detrital garnets and spinels from the Albian sediments of the Czorsztyn Unit (Pieniny Klippen Belt, Western Carpathians, Slovakia). Geologica Carpathica, **60**: 463–483.

Backert, N., Ford, M., Malartre, F., 2010. Architecture and sedimentology of the Kerinitis Gilbert-type fan delta, Corinth Rift, Greece. Sedimentology, **57**: 543–586.

Blaško, D., Nehyba, S., 2020. Synchrony evolution of two contradictory prograding Gilbert-type deltas at the margins of the foreland basin (case study from the Neogene Western Carpathian Foredeep). Marine and Petroleum Geology, **118**: 1–17.

Blum, M.D., Törnquist, T.E., 2000. Fluvial responses to climate and sea-level change. A review and look forward. Sedimentology, **47**: S1, 2–48.

Bouma, A.H., 1962. Sedimentology of Some Flysch Deposits: a Graphic Approach to Facies Interpretation. Elsevier, Amsterdam.

Breda, A., Mellere, D., Massari, F., 2007. Facies and processes in a Gilbert-delta-filled incised valley (Pliocene of Ventimiglia, NW Italy). Sedimentary Geology, **200**: 31–55.

Breda, A., Mellere, D., Massari, F., Asioli, A., 2009. Vertically stacked Gilbert-type deltas of Ventimiglia (NW Italy): the Pliocene record of an overfilled Messinian incised valley. Sedimentary Geology, **219**: 58–76.

Březina, J., Luján, Ŕ.H., Calábková, G., Ivanov, M., 2019. Revision on Historical Finding of the giant Turtle from the Brno Sand (Mliddle Miocene, Lower Badenian). Acta Musei Moraviae, Scientiae Geologicae, **103**: 113–128.

Bridge, J.S., 2003. Rivers and Floodplains. Form, Processes and Sedimentary Record. Blackwell, Oxford.

Bruhn, R., Steel, R., 2003. High-resolution sequence stratigraphy of a clastic foredeep succession (Paleocene, Spitsbergen): an example of peripheral-bulge controlled depositional architecture. Journal of Sedimentary Research, **73**: 745–755.

Brzobohatý, R., Cicha, I., 1993. Carpatnian Foredeep (in Czech with English summary). In: Geologie Moravy a Slezska (eds. A. Přichystal, V. Obstová and M. Suk): 123–128, MZM a PřF MU Brno.

Bubík, M., Petrová, P., 2004. Foraminifera of the Brno Sand in the Černovice TGB-1 borehole (in Czech with English summary). Geologické výzkumy na Moravě a ve Slezsku v roce 2004, **11**: 14–17.

Bubík, M., Nehyba, S., Petrová, P., Pospíšil, O., 2005. Miocene deposits in the HVS-2 borehole in the area of the SAKO a.s. Incinerator Plant in Brno-Líšeň (in Czech with English summary).

Geologické výzkumy na Moravě a ve Slezsku v roce 2005, **13**: 32–35.

Bubík, M., Otava, J., Hladilová, Š., 2019. Post-Palaeozoic geological history saved in sedimentary record of Miocene remnants in Brno-Líšeň (in Czech with English summary). Geologické výzkumy na Moravě a ve Slezsku v roce 2019, **26**: 16–23.

Budai, S., Colombera, L., Mountney, N.P., 2021. Quantitative characterization of the sedimentary architecture of Gilbert-type deltas. Sedimentary Geology, **426**: 106022.

Buriánek, D., Tomanová Petrová, P., Otava, J., 2012. Where do the Miocene sediments of the Brno region come from? (in Czech with English summary). Acta Musei Moraviae, Scientiae Geologicae, **97**: 153–156.

Catuneanu, O., Sweet, A.R., 1999. Maastrichtian–Paleocene foreland-basin stratigraphies, western Canada: a reciprocal sequence architecture. Canadian Journal of Earth Sciences, **36**: 685–703.

Catuneanu, O., Willis, A.J., Miall, A.D., 1998. Temporal significance of sequence boundaries. Sedimentary Geology, **121**: 157–178.

Cheel, R.J., Middleton, G.V., 1986. Horizontal lamiane formed under Upper Flow Regime Plane ded conditions. Journal of Geology, **94**: 489–504.

Chlupáč, I, Brzobohatý, R., Kovanda, J., Stráník, Z., 2002. Geologická minulost České republiky (in Czech). Academia, Praha.

Cogan, J., Lerche, I., Dorman, J.T., Kanes, W., 1993. Flexural plate inversion: application to the Carpathian Foredeep, Czechoslovakia. Modern Geology, **17**: 355–392.

Colella, A., 1988. Pliocene–Holocene fan deltas and braid deltas in the Crati Basin, Southern Italy: a consequence of varying tectonic conditions. In: Fan Deltas (eds. W. Nemec and R.J. Steel): 50–74. Blackie, Glasgow.

Collinson, J.D., Thompson, D.B., 1982. Sedimentary Structures. Allen and Unwin, London.

Čopjaková, R., 2007. The reflection of provenance changes in the psefitic and psamitic sedimentary fraction of the Myslejovice Formation (heavy mineral analysis) (in Czech). Ph.D. Thesis, Masaryk University, Brno.

Čopjaková, R., Sulovský, P., Otava, J., 2002. Comparison of the chemistry of detritic pyrope-almandine garnets of the Luleč Conglomerates with the chemistry of granulite garnets from the Czech Massif (in Czech with English summary). Geologické výzkumy na Moravě a ve Slezku v roce 2001, **9**: 44–47.

Čopjaková, R., Sulovský, P., Paterson, B.A., 2005. Major and trace elements in pyrope–almandine garnets as sediment provenance indicators of the Lower Carboniferous Culm sediments, Drahany Uplands, Bohemian Massif. Lithos, **82**: 51–70.

Dalrymple, R.W., 2004. Incised valleys in time and space: an inroduction to the volume and examination of the controls on valley formation and filling. SEPM Special Publication, **85**: 5–12.

Dietrich, P., Ghienne, J.-F., Normandeau, A., Lajeunesse, P., 2016. Upslope-migrating bedforms in a proglacial sandur delta: cyclic steps from river-derived underflows? Journal of Sedimentary Research, **86**: 113–123.

Dostalíková, L., Valentíková, H., Nehyba, S., 2018. Use of gamma-ray spectrometry for the study of Lower Badenian deposits in the borehole 2241 B Brno-Černá Pole (in Czech with English summary). Geologické výzkumy na Moravě a ve Slezsku v roce 2017, **24**: 7–12.

Edmonds, D.A., Shaw, J.B., Mohrig, D., 2011. Topset-dominated deltas: a new model for river delta stratigraphy. Geology, **39**: 1175–1178.

Eilertsen, R.S., Corner, G.D., Aasheim, O., Hansen, L., 2011. Facies characteristics and architecture related to palaeodepth of Holocene fjord-delta sediments. Sedimentology, **58**: 1784–1809.

Eliáš, M., Pálenský, P., 1998. The model for the development of the Miocene foredeeps in the Ostrava area (in Czech with English summary). Geoscience Research Reports in the year 1997: 65–66.

Elliott, T., 1989. Deltaic systems and their contribution to an understanding of basin-fill successions. Geological Society Special Publications, **41**: 3–10.

Force, E.R., 1980. The provenance of rutile. Journal of Sedimentary Research, **50**: 485–488.

Francírek, M., Nehyba, S., 2016. Evolution of the passive margin of the peripheral foreland basin: an example from the Lower Miocene Carpathian Foredeep (Czech Republic). Geologica Carpathica, **67**: 39–66.

Galloway, W.E., 1998. Siliciclastic slope and base-of-slope depositional systems: component facies, stratigraphic architecture and classification. AAPG Bulletin, **82**: 569–595.

García-García, F., Fernńndez, J., Viseras, C., Soria, J.M., 2006. Architecture and sedimentary facies evolution in a delta stack controlled by fault growth (Betic Cordillera, Southern Spain, late Tortonian). Sedimentary Geology, **185**: 79–92.

Gawthorpe, R.L., Colella, A., 1990. Tectonic controls on coarse-grained delta depositional systems in rift basins. IAS Special Publications, **10**: 113–127.

Ghinassi, M., 2007. The effects of differential subsidence and coastal topography on high-order transgressive–regressive cycles: Pliocene nearshore deposits of the Val d'Orcia Basin, Northern Apennines, Italy. Sedimentary Geology, **202**: 677–701.

Gilbert, G.K., 1885. The topographic features of lake shores. U.S. Geological Survey Annual Report, **5**: 69–123.

Gobo, K., Ghinassi, M., Nemec, W., 2014. Reciprocal changes in foreset to bottomset facies in a Gilbert-type delta: response to short-term base level changes: delta brink morphodynamics and related foreset facies. Journal of Sedimentary Research, **84**: 1079–1095.

Gobo, K., Ghinassi, M., Nemec, W., 2015. Gilbert-type deltas recording short-term baselevel changes: delta-brink morphodynamics and related foreset facies. Sedimentology, **62**: 1923–1949.

Gupta, S., 1999. Controls on sedimentation in distal margin pallaeovalleys in the Early Tertiary Alpine foreland basin, south-eastern France. Sedimentology, **46**: 357–384.

Hanžl, P., Krejčí, Z., Vít, J., Otava, J., Novák, Z., Stráník, Z., 1999. Geologická mapa Brna a okolí 1:50 000 (in Czech). Czech Geological Survey.

Haq, B.U., Hardenbol, J., Vail, P.R., 1988. Mesozoic and Cenozoic chronostratigraphy and cycles of sea-level change. SEPM Special Publication, **42**: 71–108.

Harms, J.C., Southard, J.B., Walker, R.G., 1982. Structures and sequences in clastic rocks. SEPM Short Course, **9**.

Helland-Hansen, W., Gjelberg, J.G., 1994. Conceptual basis and variability in sequence stratigraphy: a different perspective. Sedimentary Geology, **92**: 31–52.

Helland-Hansen, W., Martinsen, O.J., 1996. Shoreline trajectories and sequences: description of variable depositional-dip scenarios. Journal of Sedimentary Research, **66**: 670–688.

Hladilová, Š., Doláková, N., Nehyba, S., Hladíková, J., 2001. New results of the study of Lower Badenian sediments and fossils from some boreholes in the Carpathian Foredeep south of Brno. Geologické výzkumy na Moravě a ve Slezku v roce 2001, **9**: 31–34.

Hohenegger, J., Ćorić, S., Wagreich, M., 2014. Timing of the Middle Miocene Badenian Stage of the Central Paratethys. Geologica Carpathica, **65**: 55–66.

Holcová, K., Doláková, N., Nehyba, S., Vacek, F., 2018. Timing of Langhian bioevents in the Carpathian Foredeep and northern Pannonian Basin in relation to oceanographic, tectonic and climatic processes. Geological Quarterly, **62** (1): 3–17.

Hubert, J.F., 1962. A zircon-tourmaline-rutile maturity index and the interdependence of the composition of heavy mineral assemblages with the gross composition and texture of sandstones. Journal of Sedimentary Research, **32**: 440–450.

Hwang, I.G., Chough, S.K., 1990. The Miocene Chunbuk formation, southeastern Korea: marine Gilbert-type fan-delta system. IAS Special Publications, **10**: 235–254.

Hwang, I.G., Chough, S.K., Hong, S.W., Chee, M.Y., 1995. Controls on evolution of the fan delta systems in the Miocene Pohang Basin, SE Korea. Sedimentary Geology, **98**: 147–179.

Jervey, M.T., 1988. Quantitative Geological modeling of siliciclastic rock sequences and their seismic expression. SEPM Special Publication, **42**: 47–69.

Jiříček, R., 1987. Stratigraphy and facies subdivision of the deposits of the autochthonous Paleogene on SE slopes of the Bohe-

mian Massif (in Czech). Knihovnička Zemní Plyn a Nafta, **33**: 541–567.

Johnson, H.D., Baldwin, C.T., 1996. Shallow clastic seas. In: Sedimentary Enviroments: Processes, Facies and Stratigraphy (ed. H.G. Reading): 341–353. Blackie, London.

Kalvoda, J., Bábek, O., Fatka, O., Leichmann, J., Melichar, R., Nehyba, S., Špaček, P., 2008. Brunovistulian terrane (Bohemian Massif, Central Europe) from late Proterozoic to late Paleozoic: a review. International Journal of Earth Sciences, **97**: 497–517.

Kim, J.W., Chough, S.K., 2000. A gravel lobe deposit in the prodelta of the Doumsan fan delta (Miocene), SE Korea. Sedimentary Geology, **130**: 183–203.

Kim, S.B., Chough, S.K., Chun, S.S., 1995. Bouldery deposits in the lowermost part of the Cretaceous Kyokpori Formation, SW Korea: cohesionless debris flows and debris falls on a steep-gradient delta slope. Sedimentary Geology, **98**: 97–119.

Kostic, S., Parker, G., Marr, J.G., 2002. Role of turbidity currents in setting the foreset slope of clinoforms prograding into standing fresh water. Journal of Sedimentary Research, **72**: 353–362.

Kováč, M., Baráth, I., Harzhauser, M., Hlavatý, I., Hudáčková, N., 2004. Miocene depositional systems and sequence stratigraphy of the Vienna basin. Courier Forschunginstitut Senckenberg, **246**: 187–212.

Kováč, M., Grigorovich, A.A., Brzobohatý, R., Fodor, L., Harzhauser, M., Oszczypko, N., Pavelić, D., Rögl, F., Saftić, B., Sliva, Ľ., Stráník, Z., 2003. Karpatian paleogeography, tectonics and eustatic changes. In: The Karpatian, A Lower Miocene Stage of the Central Paratethys (eds. R. Brzobohatý, I. Cicha, M. Kováč and F. Rögl): 49–73. Masaryk University, Brno.

Krejčí, O., Ambrozek, V., Hubatka, F., Tomanová-Petrová, P., Sedlák, J., 2018. Odkrytá strukturní mapa na bázi terciérních sediment hydrogeologického rajonu 2241 a 2242 (in Czech). Czech Geological Survey.

Krystek, I., 1974. Results of the sedimentological reserch of Lower Badenian deposits in the Carpathian Foredeep (Moravia) (in Czech with English summary). Folia Facultatis Scientiarum Naturalium Universitatis Purkynianae Brunensis, Geologia, **15**: 1–32.

Krystek, I., 1984. Results of the facies and palaeogeographical study of Early Tertiary on the sw. slopes of the Bohemian Massif in segment South (in Czech with English summary). Folia Facultatis Universitatis Purkynianae Brunensis, Geologia, **24**: 1–47.

Krystek, I., Tejkal, J., 1968. Contribution to the lithology and stratigraphy of Miocene of the SW part of the Carpathian Foredeep in Moravia (in Czech with English summary). Folia přírodovědecké fakulty University J. E. Purkyně v Brně, Geologia, **9**: 1–31.

Krzywiec, P., 2001. Contrasting tectonic and sedimentary history of the central and eastern parts of the Polish Carpathian foredeep basin – results of seismic data interpretation. Marine and Petroleum Geology, **18**: 13–38.

Leszczyński, S., Nemec, W., 2015. Dynamic stratigraphy of composite peripheral unconformity in a foredeep basin. Sedimentology, **62**: 645–680.

Longhitano, S.G., 2008. Sedimentary facies and sequence stratigraphy of coarse-grained Gibert-type deltas within the Pliocene thrust-top Potenza Basin (Southern Apennines, Italy). Sedimentary Geology, **210**: 87–110.

López-Blanco, M., Marzo, M., Piña, J., 2000. Transgressive–regressive sequence hierarchy of foreland, fan-delta clastic wedges (Montserrat and Sant Llorenç del Munt, Middle Eocene, Ebro Basin, NE Spain). Sedimentary Geology, **138**: 41–69.

Lowe, D.R., 1982. Sediment gravity flows: II. Depositional models with special reference to the deposits of high-density turbidity currents. Journal of Sedimentary Petrology, **52**: 279–297.

Mange, M.A., Morton, A.C., 2007. Geochemistry of heavy minerals. In: Heavy Minerals in Use. Developments in Sedimentology, **58**: 345–391.

Martini, I., Ambrosetti, E., Sandrelli, F., 2017. The role of sediment supply in large-scale stratigraphic architecture of ancient Gilbert-type deltas (Pliocene Siena-Radicofani Basin, Italy). Sedimentary Geology, **350**: 23–41.

Massari, F., 1996. Upper-flow-regime stratification types on steep-face, coarse-grained, Gilbert-type progradational wedges (Pleistocene, southern Italy). Journal of Sedimentary Research, **66**: 364–375.

Massari, F., Colella, A., 1988. Evolution and types of fan-delta systems in some major tectonic setting. In: Fan Deltas (eds. W. Nemec and R.J. Steel): 101–122. Blackie and Son, London.

Massari, F., Parea, G.C., 1990. Wave-dominated Gilbert-type gravel deltas in the hinterland of the Gulf of Taranto (Pleistocene, southern Italy). IAS Special Publications, **10**: 311–331.

Meinhold, G., Anders, B., Kostopoulos, D., Reischmann, T., 2008. Rutile chemistry and thermometry as provenance indicator: an example from Chios Island, Greece. Sedimentary Geology, **203**: 98–111.

Miall, A.D., 1996. Principles of Sedimentary Basin Analysis. Springer, New York.

Miller, K.G., Mountain, G.S., Browning, J.V., Kominz, M., Sugarman, P.J., Christie-Blick, N., Katz, M.E., Wright, J.D., 1998. Cenozoic global sea level, sequences, and the New Jersey Transect: results from coastal plain and continental slope drilling. Reviews of Geophysics, **36**: 569–601.

Mortimer, E., Gupta, S., Cowie, P., 2005. Clinoform nucleation and growth in coarse grained deltas, Loreto basin, Baja California Sur, Mexico: a response to episodic accelerations in fault displacement. Basin Research, **17**: 337–359.

Morton, A.C., 1984. Stability of detrital heavy minerals in Tertiary sandstones from the North Sea Basin. Clay Minerals, **19**: 287–308.

Morton, A.C., Hallsworth, C.R., 1994. Identifying provenance-specific features of detrital heavy mineral assemblages in sandstones. Sedimentary Geology, **90**: 241–256.

Mulder, T., Alexander, J., 2001. The physical character of subaqueous sedimentary density flows and their deposits. Sedimentology, **48**: 269–299.

Muto, T., Steel, R.J., 1997. Principles of regression and transgression: the nature of the interplay between accommodation and sediment supply. Journal of Sedimentary Research, **67**: 994–1000.

Nehyba, S., 2018. Lower Badenian coarse-grained Gilbert deltas in the southern margin of the Western Carpathian Foredeep basin. Geologica Carpathica, **69**: 89–113.

Nehyba, S., Roetzel, R., 2010. Fluvial deposits of the St. Marein-Freischling Formation – insights into initial depositional processes on the distal external margin of the Alpine-Carpathian Foredeep in Lower Austria. Austrian Journal of Earth Sciences, **103**: 50–80.

Nehyba, S., Šikula, J., 2007. Depositional architecture, sequence stratigraphy and geodynamic development of the Carpathian Foredeep (Czech Republic). Geologica Carpathica, **58**: 53–69.

Nehyba, S., Roetzel, R., Adamová, M., 1999. Tephrostratigraphy of the Neogene volcaniclastics (Moravia, Lower Austria, Poland). Geologica Carpathica, **50** (Spec. Iss.): 126–128.

Nehyba, S., Tomanová Petrová, P., Zágoršek, K., 2008. Sedimentological and palaeocological records of the evolution of the south-western part of the Carpathian Foredeep (Czech Republic) during the Early Badenian. Geological Quarterly, **52** (1): 45–60.

Nehyba, S., Holcová, K., Gedl, P., Doláková, N., 2016. The Lower Badenian transgressive-regressive cycles – a case study from Oslavany (Carpathian Foredeep, Czech Republic). Neues Jahrbuch für Geologie und Paläontologie – abhandlungen, **279**: 209–238.

Nehyba, S., Gilíková, H., Tomanová-Petrová, P., Otava, J., Skácelová, Z., 2019. Evolution of a sedimentary infill of a palaeovalley at a distal margin of the peripheral foreland basin. Geological Quarterly, **63** (2): 319–344.

Nemec, W., 1990. Aspects of sediment movement on steep delta slope. IAS Special Publications, **10**: 29–73.

Nemec, W., 1995. The dynamics of deltaic suspension plumes. In: Geology of Deltas (eds. M.N. Oti and G. Postma): 31–93. Balkema, Rotterdam, NT.

Nemec, W., Steel, R.J., Porebski, S.J., Spinnangr, A., 1984. Domba conglomerate, Devonian, Norway: process and lateral variability in a mass flow-dominated, lacustrine fandelta. Canadian Society of Petroleum Geologists Memoir, **10**: 295–320.

Nemec, W., Lønne, I., Blikra, L.H., 1999. The Kregnes moraine in Gauldalen, west-central Norway: anatomy of a Younger Dryas proglacial delta in a palaeofjord basin. Boreas, **28**: 454–476.

Okazaki, H., Isaji, S., Kurozumi, T., 2020. Sedimentary facies related to supercritical-flow bedforms in foreset slopes of a Gilbert-type delta (middle Peistocene, central Japan). Sedimentary Geology, **399**.

Oszczypko, N., Krzywiec, P., Popadyuk, I., Peryt, T., 2006. Carpathian Foredeep Basin (Polish and Ukraine): its sedimentary, structural, and geodynamic evolution. AAPG Memoir, **84**: 293–350.

Otava, J., Sulovský, P., Čopjaková, R., 2000. Provenance changes of the Drahany Culm greywackes: statistical evaluation. (in Czech), Geologické výzkumy na Moravě a ve Slezku v roce 1999: 94–98.

Papp, A., Cicha, I., Seneš, J., Steininger, F., 1978. Chronostratigraphie und neostratotypen, Miozän der Zentralen Paratethys, 4, M4 Badenian (Moravien, Wielicien, Kosovien). Bratislava (Veda).

Petrová, P., 2004. Foraminiferal assemblages as an indicator of foreland basin evolution (Carpathian Foredeep, Czech Republic). Bulletin of Geosciences, **79**: 231–242.

Pícha, F.J., 1979. Ancient submarine canyons of Tethyan continental margins, Czechoslovakia. AAPG Bulletin, **63**: 67–86.

Pícha, F.J., Stránik, Z., Krejčí, O., 2006. Geology and hydrocarbon resources of the Outer Western Carpathians and their foreland, Czech Republic. AAPG Memoir, **84**: 49–175.

Plink-Björklund, P., Ronnert, L., 1999. Depositional processes and internal architecture of Late Weichselian ice-margin submarine fan and delta settings, Swedish west coast. Sedimentology, **46**: 215–234.

Postma, G., 1984. Mass-flow conglomerates in a submarine canyon: abrioja fan delta, Pliocene, Southeast Spain. Canadian Society of Petroleum Geologists Memoir, **10**: 237–258.

Postma, G., 2001. Physical climate signatures in shallow and deep-water deltas. Global and Planetary Change, **28**: 93–106.

Postma, G., Cruickshank, C., 1988. Sedimentology of a late Weichselian to Holocene, terraced fan delta, Varangerfjord, northern Norway. In: Fan Deltas (eds. W. Nemec and R.J. Steel): 144–157. Blackie and Son.

Poulimenos, G., Zelilidis, A., Kontopoulos, N., Doutsos, T., 1993. Geometry of trapezoidal fan deltas and their relationship to extensional faulting along the southwestern active margins of the Corinth rift, Greece. Basin Research, **5**: 179–192.

Powers, M.C., 1982. Comparison chart for estimating roundness and sphericity. AGI Data Sheet 18.

Rasmussen, H., 2000. Nearshore and alluvial facies in the Sant Llorenç del Munt depositional system: recognition and development. Sedimentary Geology, **138**: 71–98.

Rubi, R., Rohais, S., Bourquin, S., Moretti, I., Desaubliaux, G., 2018. Processes and typology in Gilbert-type delta bottomset deposits based on outcrop examples in the Corinth Rift. Marine and Petroleum Geology, **92**: 193–212.

Russell, A.J., 2007. Controls on the sedimentology of an ice-contact jökulhlaup-dominated delta, Kangerlunssuaq, west Greenland. Sedimentary Geology, **193**: 137–148.

Shanley, K.W., McCabe, P.J., 1994. Perspectives on the sequence stratigraphy of continental strata. AAPG Bulletin, **78**: 544–568.

Smith, N.D., 1974. Sedimentology and bar formation in the upper Kicking Horse River, a braided outwash stream. Journal of Geology, **81**: 205–223.

Sohn, Y.K., Kim, S.B., Hwang, I.G., Choe, M.Y., Chough, S.K., 1997. Characteristic and depositional processes of large-scale gravelly Gilbert-type foresets in the Miocene Doumsan fan delta, Pohang basin, SE Korea. Journal of Sedimentary Research, **67**: 130–141.

Steel, R.J., Olsen, T., 2002. Clinoforms, clinoform trajectories and deepwater sands. GCS-SEPM Special Publication: 367–361.

Talling, P.J., Masson, D.G., Sumner, E.J., Malgesini, G., 2012. Subaqueous sediment density flows: depositional processes and deposit types. Sedimentology, **59**: 1937–2003.

Tolosana-Delgado, R., von Eynatten, H., Krippner, A., Meinhold, G., 2018. A multivariate discrimination scheme of detrital garnet chemistry for use in sediment provenance analysis. Sedimentary Geology, **375**: 14–26.

Tomanová-Petrová, P., Švábebnická, L., 2007. Lower Badenian biostratigraphy and paleoecology: a case study from the Carpathian Foredeep (Czech Republic). Geologica Carpathica, **58**: 333–352.

Triebold, S., Eynatten, H. von, Luvizotto, G.L., Zack, T., 2007. Deducing source rock lithology from detrital rutile geochemistry: an example from the Erzgebirge, Germany. Chemical Geology, **244**: 421–436.

Triebold, S., Eynatten H. von, Zack, T., 2012. A recipe for the use of rutile in sedimentary provenance analysis. Sedimentary Geology, **282**: 268–275.

Tucker, M. 1995. Techniques in Sedimentology. Blackwell Science, Oxford.

Turmel, D., Locat, J., Parker, G., 2015. Morphological evolution of a well-constrained, subaerial–subaqueous source to sink system: Wabush Lake. Sedimentology, **62**: 1636–1664.

Ventra, D., Cartigny, M.J.B., Bijkerk, J.F., Acikalin, S., 2015. Supercritical-flow structures on a Late Carboniferous delta front: sedimentological and paleoclimatic significance. Geology, **43**: 731–734.

Viparelli, E., Blom, A., Parker, G., 2012. Modeling stratigraphy formed by prograding Gilbert deltas. In: River Flow 2012 (ed. E. Murillo): 827–836. Taylor and Francis Group, London.

Viseras, C., Calvache, M.L., Soria, J.M., Fernandez, J., 2003. Differential features of alluvial fans controlled by tectonic or eustatic accommodation space. Examples from the Betic Cordillera, Spain. Geomorphology, **50**: 181–202.

Walker, R.G., James, N.P., 1992. Facies Models: Response to Sea Level Changes. Geological Association of Canada, St. John's.

Wang, R., Colombera, L., Mountney, N.P., 2019. Geologic controls on the geometry of incised-valley fills:Insights from a global dataset of late-Quaternary examples. Sedimentology, **66**: 2134–2168.

Waschbusch, P.J., Royden, L.H., 1992. Spatial and temporal evolution of foredeep basins: lateral strength variations and inelastic yielding in continental lithoshere. Basin Research, **4**: 179–196.

Watson, E., Wark, D., Thomas, J., 2006. Crystallization thermometers for zircon and rutile. Contributions to Mineralogy and Petrology, **151**: 413–433.

Weleschuk, Z.P., Dashtgard, S.E., 2019. Evolution of an ancient (Lower Cretaceous) marginal-marine system from tide-dominated to wave-dominated deposition, McMurray Formation. Sedimentology, **66**: 2354–2391.

Zack, T., Eynatten, H. von, Kronz, A., 2004a. Rutile geochemistry and its potential use in quantitative provenance studies. Sedimentary Geology, **171**: 37–58.

Zack, T., Moraes, R., Kronz, A., 2004b. Temperature dependence of Zr in rutile: empirical calibration of a rutile thermometer. Contributions to Mineralogy and Petrology, **148**: 471–488.

Zaitlin, B.A., Dalrymple, R.W., Boyd, R., 1994. The stratigraphic organization of incised-valley systems associated with relative sea-level change. SEPM Special Publication, **51**: 45–60.

Zavala, C., Arcuri, M., 2016. Intrabasinal and Extrabasinal turbidites: origin and distinctive characteristics. Sedimentary Geology, **337**: 36–54.

Zelilidis, A., Kontopoulos, N., 1996. Significance of fan deltas without toe-sets within rift and piggy-back basins: examples from the Corinth graben and the mesohellenic trough, Central Greece. Sedimentology, **43**: 253–262.

Zingg, T., 1935. Beitrag zur Schotteranalyse. Die Schotteranalyse und ihre Anwendung auf die Glattalschotter. Schweizerische Mineralogische und Petrographische Mitteilungen, **15**: 39–140.